This manuscript is a non-peer-reviewed preprint submitted to EarthArXiv. The manuscript has been submitted to Sedimentologika for publication. Depending on the peer-review process, the content of the manuscript may change. If accepted, the final version of this manuscript will be available via the DOI link of the peer-reviewed publication.

Interplay between subsidence and sediment flux in the filling of the North Pyrenean retro-foreland basin during the Eocene (Corbières, France)

Marine Prieur^{1*}, Justine Briais² and Eric Lasseur²

- ¹ Department of Earth Sciences, University of Geneva, Switzerland
- ² BRGM, Orléans, France
- * m.prieur.t@gmail.com

Abstract

External forcings, such as climate and tectonics, influence sedimentary basin fills. In turn, sedimentary archives provide key information on variations in accommodation and sediment flux over time, which record paleoclimate and tectonic conditions. However, the impacts of accommodation and flux on sedimentation must be disentangled before understanding their specific influence on surface processes. This study focuses on the Talairan Syncline (Corbières area, France) in the northeastern Pyrenean retro-foreland during the Early Eocene. This basin is filled with continental deposits coeval with the initiation of the major tectonic pulse of the Pyrenean orogeny and the Early Eocene Climatic Optimum. Therefore, the Talairan Syncline enables the characterization of the impact of flux and subsidence on the filling of a tectonically active area during climate changes. Detailed mapping and facies analyses led to the identification of four depositional sequences marked by clear erosional surfaces and syn-tectonic growth strata. The evolution of the stratigraphy over time indicates a progradation of the gravel front, accompanied by a net decrease in the downstream grain size fining rate. This change is linked to an enhanced imprint of sedimentary flux on sedimentation compared to subsidence. These results suggest a clear influence of subsidence in the early stages of the North Pyrenean retro-foreland's development, followed by an increased influence of flux, resulting in a larger depositional area and an increased export of sediments downstream. Referencing these settings enables the identification of the interplay between subsidence and flux over time, paving the way for further studies to define the impact of climate and tectonics on flux variations.

Lay summary

Changes in climate and tectonics influence how sediments are deposited in sedimentary basins. The challenge is to interpret past variations in climate and tectonics, and their impact on sedimentation, to disentangle the effects of each of these environmental factors. In this study, we focus on the syn-orogenic terrestrial series of the Talairan Basin fill, located in the northeastern piedmont of the Pyrenees. Sedimentation in this basin occurred during the Early Eocene, a period of high tectonic activity in the Pyrenees and significant climate change. The mapping of geological units and descriptions of the nature of the sedimentary rocks over time allowed us to reconstruct the basin's filling history. We shed light on strong tectonic imprints, suggesting that subsidence played a role in the sediment deposition. Then, studying the grain size of the fluvial sediments, we calculated the fining rate downstream from the mountain front along the successive sequences. The decreasing grain size fining rate over time suggests a greater influence of sediment and water fluxes on sedimentation processes compared to subsidence for the last stage of the Talairan Basin fill. Therefore, our results suggest that the basin was initially shaped by intense tectonics related to the Pyrenean orogeny, followed by increases in flux over subsidence, leading to basin filling and the export of sediments farther from the mountain front. This case study illustrates how tectonics and flux influence the development of a syn-orogenic frontal basin fill, paving the way for further studies on the specific impact of climate and tectonics on the observed increase in flux.

Résumé

Le remplissage des bassins sédimentaires est influencé par des facteurs externes que sont le climat et la tectonique. Les archives sédimentaires fournissent donc des informations clés sur les variations du taux d'accommodation et du flux sédimentaire dans le temps, qui reflètent les paléoclimats et conditions tectoniques. Cependant, les impacts du climat et de la tectonique doivent être distingués avant d'étudier l'influence de chacun de ces facteurs sur les processus sédimentaires. Cette étude porte sur le synclinal de Talairan (Corbières, France), situé dans la partie est du bassin nord-pyrénéen de type rétro-foreland, à l'Éocène. Ce remplissage continental, synchrone avec une phase tectonique intense et un maximum thermique appelé Early Eocene Climatic Optimum, permet d'identifier l'impact du flux et de la subsidence sur les dynamiques sédimentaires d'un bassin tectoniquement actif lors d'un

changement climatique majeur. Une cartographie détaillée de la zone et des descriptions de faciès ont permis d'identifier quatre séquences de dépôt, marquées par des troncatures d'érosion et des discordances progressives. La stratigraphie montre, au cours du temps, une progradation de la limite gravier-sable et une diminution nette du taux de décroissance granulométrique vers l'aval, ce qui indique une augmentation de l'influence du flux par rapport à la subsidence. Ces résultats indiquent une influence marquée de la subsidence au début du remplissage du bassin nord-pyrénéen, suivie d'une influence accrue du flux, reflétée par une zone de dépôt plus étendue et par un export sédimentaire plus conséquent vers l'aval. Cela permet d'identifier l'interaction entre subsidence et flux au cours du temps dans le remplissage d'un bassin d'avant-pays frontal, ouvrant la voie à des études sur le rôle du climat et de la tectonique dans cette augmentation du flux.

Key words - Climate, Tectonics, Pyrenees, EECO, Grain size fining

1. Introduction

The piedmont and alluvial plain areas are part of the terrestrial transfer zone of a sedimentary system, where sediments, eroded from the mountainous catchment, are partially deposited and partially transported to the oceanic sink (Romans et al., 2016; Tofelde et al., 2021). The amount of sediments stored in the transfer zone depends on (1) the tectonic setting, through the rates and repartition of subsidence or uplift, and (2) the sedimentary flux (Qs), dictating the quantity of sediments input to the basin (Allen et al., 2013). Qs is itself impacted by the tectonic-induced catchment area and by climate-related water discharge and erosion rates (Allen et al., 2013). Subsidence and Qs therefore impact sediment dispersal, which is primarily recorded in the transfer zone, located at the exit of the catchment. The mode of sediment transfer in the alluvial plain and the grain size segregation rates inform on the propagation of tectonic and climatic perturbations along a sedimentary system (Armitage et al., 2011; Paola et al., 1992; Whittaker et al., 2011). However, before interpreting the effect of tectonics and climate on sedimentation, we need to decipher the relative influences of subsidence and flux.

Tectonic influence on sedimentation can be directly identified from erosional features and growth strata. Yet, apart from these direct tectonic features, the identification of subsidence and flux impact on sedimentary fills is indirect, as both subsidence and aggradation impact sedimentation rates. This is particularly the case in continental series, where the continental slope varies in response to changes in sediment flux and water discharge (Armitage et al., 2011; Simpson & Castelltort, 2012). The size of the sedimentary system is also influenced by both subsidence and sediment flux, and the role played by each is difficult to estimate. Finally, grain size and the downstream fining rate of continental deposits can serve to quantify the influence of subsidence and flux on deposition (Whittaker et al., 2011). Therefore, applying these methods to a continental basin fill can serve to identify the competing impacts of subsidence and flux.

During the Eocene, the North Pyrenean retro-foreland basin recorded important deformation in the Corbières area (France) due to the Pyrenean orogeny (Christophoul et al., 2003). The Early Eocene is a period of orogenic growth in the Pyrenees, as indicated by shortening rates (Verges et al., 1995), the cooling history of the granitic massifs (Ternois et al., 2019), and increased subsidence in the North Pyrenean retro-foreland (Ford et al., 2022). Located in the eastern part of the retro-foreland, at the foothill of the Mouthoumet Thrust, the Talairan Syncline formed during the Early Eocene. It is filled by continental conglomeratic series belonging to the First Unit of the Palassou Formation and assigned to piedmont sedimentation derived from the growing Pyrenean orogen. Eocene syn-tecto-

nic sedimentation features are identified by Christophoul et al. (2003) and Martín-Martín et al. (2001) in the Corbières area.

Therefore, the infill of the Talairan Syncline was likely influenced by both subsidence and sedimentary flux. However, although it exhibits a wide diversity of facies, ranging from proximal fluvial channels to lacustrine deposits, the internal composition of the Palassou First Unit has never been documented or questioned in terms of external forcing during the early growth of the orogen and correlative frontal basin development.

In this study, we provide detailed descriptions of the sedimentary facies, stratigraphic geometry, geological mapping, and log correlation of the Palassou First Unit in the Talairan Syncline. Then, we conduct grain size analyses for each of the four stratigraphic sequences described to calculate downstream fining rates and discuss the impact of flux and subsidence on each stage of the basin fill.

2. Geological setting

The Pyrenees formed as a result of the collision between the Iberian and European plates from the Late Cretaceous to the Oligocene. The present structure is composed of a Paleozoic Axial Zone, which is flanked to the north and the south by highly deformed Mesozoic strata, remnants of the Early Cretaceous rifting (Figure 1A). Given the double-wedge structure of the orogeny (Roure et al., 1989), frontal thrusts separate the North and South Pyrenean Zones, forming the fold-and-thrust belts of the Aquitaine and Ebro basins from the Mesozoic to the Cenozoic (Figure 1A). The frontal thrusts result from the inversion of normal faults related to the Early Cretaceous rift (Baby et al., 1988; Beaumont et al., 2000; Vauchez & Barruol, 1996). The orogeny began during the Late Cretaceous and was followed by a period of relative quiescence during the Paleocene (Angrand & Mouthereau, 2021; Ford et al., 2022). An acceleration of the orogenic growth and compression occurred at the Early Eocene in the eastern Pyrenees (Ford et al., 2016; Ford et al., 2022; Ternois et al., 2019) and propagated westward due to rift-inherited variations in the lithosphere (Sinclair & Naylor, 2012; Teixell et al., 2016). The Pyrenean compression ended by the late Oligocene to the early Miocene (Rosenbaum et al., 2002).

The Corbières area is located to the northeast of the Pyrenees, between the North Pyrenean Frontal Thrust (NPFT) and Mouthoumet Thrust in the south, and the Montagne Noire, part of the Massif Central craton in the north (Figure 1B). The frontal basins located to the north of the frontal thrust are presently segmented in synclines filled with syn-orogenic Palassou series

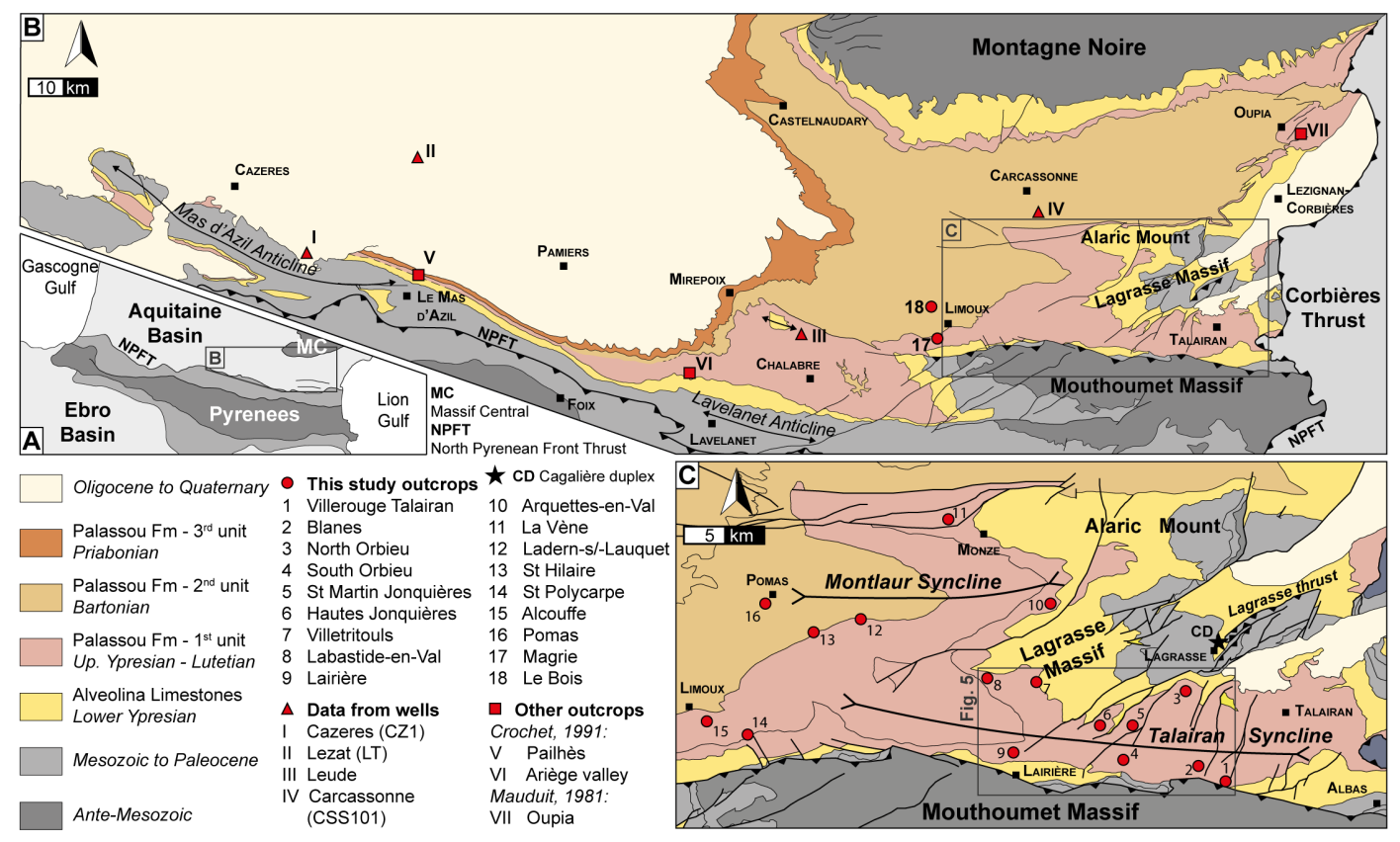


Figure 1: Geological map of the Corbières area. (A) The Pyrenean fold-and-thrust belt is located between the Aquitaine and Ebro foreland basins. (B) Geology of the north-eastern foreland, with detailed mapping of the three units of the Palassou Formation. (C) Zoom in on the Talairan Syncline area, where the square indicates the location of the detailed map shown in Figure 5. The data used are indicated as red dots, triangles, or squares depending on whether they come from this study, wells, or other studies. (Geological maps are modified from BRGM).

and limited by anticlines of deformed Lower Ypresian and Mesozoic formations (Figure 1B). In the studied area, the Talairan Syncline, Montlaur Syncline, and Carcassonne Basin are separated by the Lagrasse Massif, which comprises numerous internal deformations and thrusting (Souque et al., 2003), and the Alaric Mount (Figure 1C).

The NPFT and the Mouthoumet Thrust were active during the first compressional event from late Campanian to Maastrichtian (Durand-Delga & Charrière, 2012; Ford et al., 2016; Tambareau et al., 1995; Ternois et al., 2019; Vinciguerra, 2020). Associated deposits show very shallow marine environments (Tambareau et al., 1995), fed primarily by the Sardinia block to the east and secondarily by the Massif Central craton in the north (Ternois, 2019; Vinciguerra, 2020). The Paleocene tectonic quiescence (Angrand & Mouthereau, 2021; Ford et al., 2022) is recorded by Danian and Selandian alluvial shales and lacustrine limestones lying unconformably over the Late Cretaceous strata (Maufrangeas et al., 2020; Tambareau et al., 1995). From the Thanetian, the Pyrenees are the main feeder of the basin (Plaziat, 1981), marked mainly by terrestrial successions (Tambareau et al., 1995; Vinciguerra, 2020) with three marine transgressions (Tambareau et al., 1995). Following the large-scale marine transgression at the lowermost Ypresian with the deposition of the Ilerdian alveolina-rich carbonate shelf, northward delta progradation led to continental deposits (Christophoul et al., 2003; Martín-Martín et al., 2001; Plaziat, 1981; Tambareau et al., 1995) from the Lower Ypresian (SBZ 8-9) (Berger et al., 1997; Christophoul et al., 2003; Crochet, 1991). During the Eocene, the main collision phase of the Pyrenees (Ford et al., 2016; Ford et al., 2022; Ternois et al., 2019) led in the Corbières area to the reactivation of the NPFT and the Mouthoumet Thrust, along with the activation of the Lagrasse, Alaric, and Oupia faults (Averbuch et al., 1992; Christophoul et al., 2003).

The Upper Ypresian to Priabonian continental molasse deposited in the eastern Aquitaine Basin comprises fluvial and lacustrine deposits grouped in the Palassou Formation (Crochet, 1991). The Palassou Formation is divided into three units, with lacustrine intervals at the top of each. The presence of mollusk shells and mammal rodents suggests an Upper Ypresian to Lutetian age for the First Unit, a Bartonian age for the Second Unit, and a Priabonian age for the Third Unit (Crochet, 1991). The syn-tectonic Palassou Formation (Christophoul et al., 2003; Crochet, 1991; Martín-Martín et al., 2001) shows an evolution of conglomeratic clasts' lithology, with the First Unit dominated by Mesozoic and Cenozoic rock fragments and the Second Unit marked by the appearance of granitic clasts, suggesting a change in the source area, reaching the North Pyrenean granites and the Axial Zone (Al Reda et al., 2021; Crochet, 1991).

During the Palassou First Unit occurred the Early Eocene Climate Optimum (EECO) (Greenwood & Wing, 1995; Lauretano et al., 2015; Pearson et al., 2001; Zachos et al., 2001; Zachos et al., 2005), defined from ~53 to ~51 Ma by a negative shift in the stable carbon isotopic records marked by successive hyperthermals (Cramer et al., 2009; Lauretano et al., 2016; Zachos et al., 2008; Zachos et al., 2001). This period is marked by a hothouse climate (Westerhold et al., 2020) with high temperatures, as suggested by the oxygen isotopic curves from ~53 to ~47 Ma (Cramer et al., 2009; Luciani et al., 2016; Westerhold et al., 2020; Westerhold et al., 2018; Zachos et al., 2001). In the Southern Pyrenees, the hyperthermals associated with the EECO correlate with enhanced sediment transport due to enhanced

precipitation, which is marked by increased sediment flux and water discharge in the fluvial Castissent Formation (Honegger et al., 2020; McLeod et al., 2025) and successive progradation of the deltaic Castigaleu Formation (Vaucher et al., 2024). On the northern side of the Pyrenees, at the foothill of the Montagne Noire (Figure 1), the EECO led to enhanced sediment flux due to monsoon-like changes in precipitation (Boyrie et al., 2025), in time-equivalent deposits of the Palassou First Unit. However, the impact of the EECO on the North-Pyrenean catchments was never discussed. A more detailed definition of the composition and stratigraphy of the Palassou First Unit is necessary to discuss the impact of climate and tectonics on its deposition.

3. Methods

3.1. Facies analysis and sequence stratigraphy

The fieldwork description of 18 sedimentary logs through the Palassou First Unit in the Corbières area, including 9 in the Talairan Syncline (Figure 1), led to the identification of 11 facies and 8 facies associations, which were used to interpret depositional environments. The stratigraphy of each log is then studied using the concept of sequence stratigraphy, based on the ratio between accommodation (A) and sediment flux (S). Within continental basin fill, progradation trends (decreasing A/S) are characterized by coarser deposits and decreasing rates of floodplain preservation, linked to an increase in channel frequency and amalgamation (Cain & Mountney, 2009; Owen, Ebinghaus, et al., 2017; Owen, Nichols, et al., 2017; Shanley & McCabe, 1991; Weissmann et al., 2015). The maximum prograding surface (PM) corresponds to the coarser sediments or the highest amalgamation rate (Olsen et al., 1995; Shanley & McCabe, 1994; Steel & Ryseth, 1990). Retrograding trends are identified by deposits becoming more fine-grained up section, linked to an increasing proportion of floodplain being deposited and preserved, and fluvial channels becoming more isolated, with smaller dimensions, and filled by finer sediments (Owen, Nichols, et al., 2017). The maximum retrograding surface (RM) is defined by laterally continuous marine or lacustrine deposits (Olsen et al., 1995; Owen, Nichols, et al., 2017; Shanley & McCabe, 1991, 1994; Shanley et al., 1992) or a relatively thick accumulation of floodplain deposits in a more proximal area (Owen, Nichols, et al., 2017).

The end of the early Ypresian deltaic deposits (Martín-Martín et al., 2001; Plaziat, 1981; Tambareau et al., 1995) serves as a datum for the correlation, corresponding to an age of ~53 Ma from the nannofossil zone NP11-12 and shallow benthic foraminifers zone SBZ8-9 (Christophoul et al., 2003; Martín-Martín et al., 2001). The transition from deltaic to continental deposits is considered quasi-synchronous over the Talairan Syncline. Given the apparent complexity of the area, once vertical trends were identified in representative sections, precise mapping was done to follow sedimentary packages and correlate main surfaces.

3.2. Geological mapping and photogrammetry

Available geological maps of the Corbières area, specifically in the Talairan Syncline, distinguish the three units of the Palassou Formation (Berger et al., 1997; Crochet et al., 1989; Ellenberger et al., 1985). Yet, this study provides an accurate geological map of the First Unit to inform on lateral facies variations. We defined 12 sedimentary packages or members coupled to dip measurements and paleocurrents to inform on structural and sedimentary features within the Talairan Syncline.

Over the last forty years, increased vegetation cover in the Corbières area has made mapping difficult. We used open-access aerial photographs from 1976, with a mean scale of 1:20,000 (remonterletemps.ign.fr) and a one-third overlap, to generate a 3D georeferenced model using the photogrammetry software Agisoft Metashape Professional and following the image-based rendering method (Figure S1) (El Garouani et al., 2014; Remondino & El-Hakim, 2006). We utilized the past low-vegetation-cover model to precisely delineate the horizons and identify any manifestation of syn- and post-sedimentary tectonics. Indeed, the evolution of dips over the area helped to highlight abnormal contacts between two horizons (Figure S1). Combining facies analyses, sequence stratigraphy, and geological mapping provides a qualitative description of the Palassou First Unit stratigraphy in the Talairan Syncline.

3.3. Grain size analysis

Grain size measurements in fluvial conglomeratic beds are conducted over the Talairan Syncline to quantify sedimentary processes within the established stratigraphy. Grain size is measured on 32 conglomerate bodies from scaled photographs corrected for distortion (Garefalakis et al., 2023; Storz-Peretz & Laronne, 2013). Median grain size (D $_{\rm 50}$) and the 84th percentile (D $_{\rm 84}$) are calculated from bulk measurement of around 1000 pebbles, accounting for the maximum apparent axis of pebbles larger than 2mm (Garefalakis et al., 2023).

The downstream grain size fining rate is estimated to inform the interplay between subsidence and sediment flux (Armitage et al., 2011; Robinson & Slingerland, 1998; Whittaker et al., 2011). For each of the four depositional sequences, 6 to 13 grain size data are plotted with radial distance to an estimated apex. In the long term, grain size fining rate depends on (1) the grain size and flux of input sediment supply, (2) the spatial distribution of subsidence, and (3) the sediment transport dynamics (Armitage et al., 2011; Duller et al., 2010; Fedele & Paola, 2007; Hoey & Bluck, 1999; Robinson & Slingerland, 1998; Whittaker et al., 2011). Coarse-grain down-system fining in a closed system usually follows an exponential Sternberg equation:

$$D_p(x) = D_{p0}.e^{-\alpha x}$$

with x the distance from the apex (i.e., the outlet from mountainous catchment, in km), D_{p0} the predicted grain size of percentile p at the apex (in mm), and α the predicted fining exponent (in km⁻¹) (e.g., Robinson & Slingerland, 1998). The input grain size and fining exponent are determined and compared for each stratigraphic sequence.

4. Results

4.1. Sedimentary facies

Facies and facies associations (F1 to F11 and A1 to A8) represent fluvial channel, floodplain, and lacustrine environments. Succinctly described below, the extensive facies description tables are provided in the Supplementary Materials (Tables S1 and S2). Figure 2 illustrates the facies associations, and we

mention their occurrence in the logs (L1 to L9; Figure S2) and mapped formations (Figure 4).

Fluvial channel facies associations

Amalgamated conglomeratic channels (A1; Figure 2A) are

the most proximal facies association, observed through large, erosive, and thick bodies (up to tens of meters) composed of coarse-grained and poorly sorted conglomerates (F6). Successive channel erosions and large foresets can be distinguished (F11), although the coarseness of the deposits sometimes makes those structures hardly recognisable (F7; Allen, 1981; Hartley

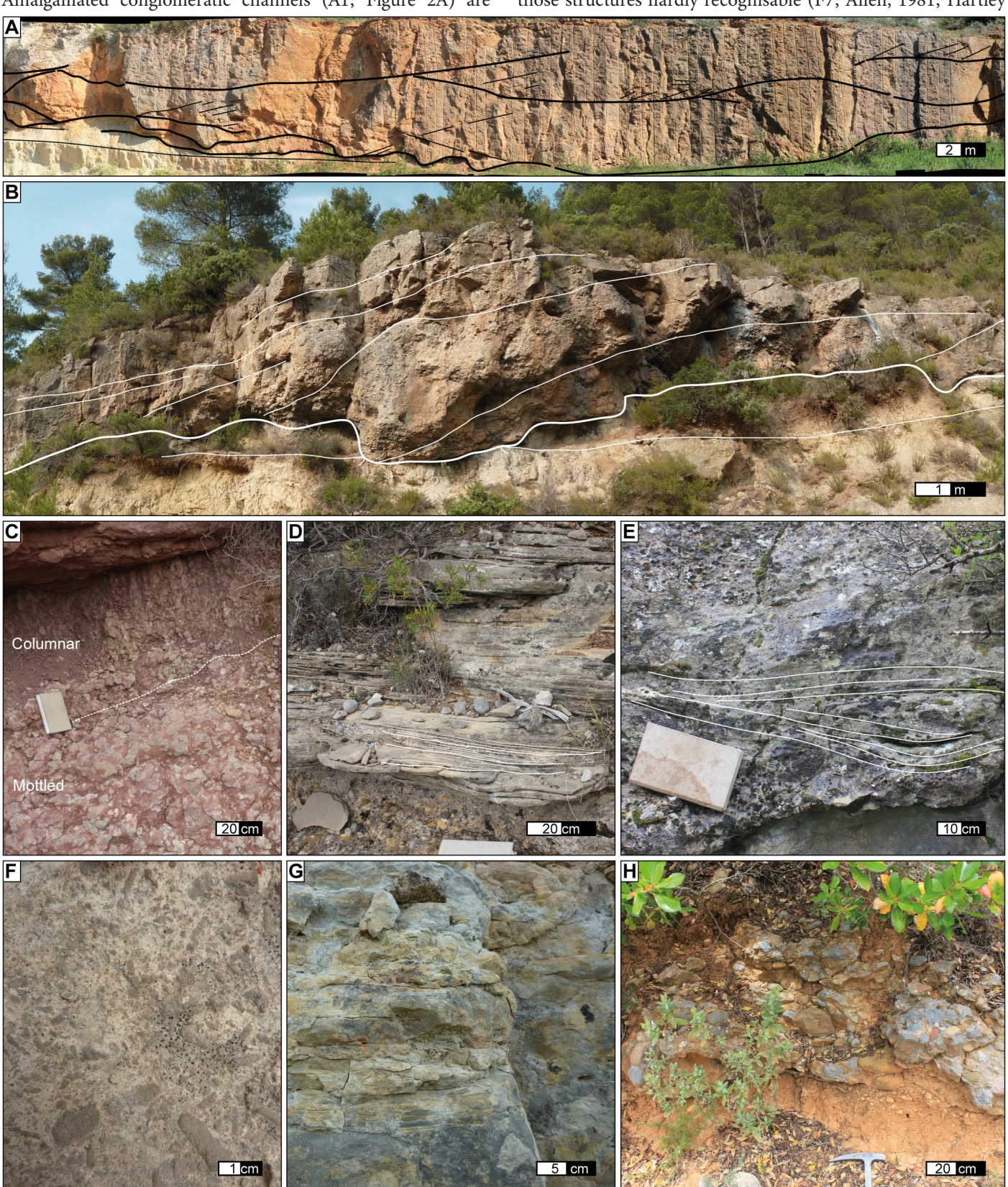


Figure 2: Facies illustrations. (A) A1: Amalgamated conglomeratic bodies with channel scours and foresets. (B) A2: Isolated channel with large foresets (F11), eroding floodplain deposits (A5). (C) Alluvial plain deposits (A5): hydromorphic paleosol in the lower part (F2) and paleosol in the upper part (F1). (D) Sandy megaripples (F10) on top of a conglomeratic channel (A3). (E) Humpback cross bedding amongst sand to pebble poorly sorted bodies (F8). (F) Abundant algae in a very fine sandstone (F3) showing a lake environment (A6). (G) Lacustrine packstone (F3; A6). (H) Thin sheet of unsorted conglomerates (F6) found within lacustrine deposits (A8).

et al., 2015). Amalgamated conglomeratic channels are visible markers in the Talairan Syncline landscape, composing the Blanes and Viala Conglomerates, as well as at the basal Flowers Formation (L2, L3, L4, and L9).

Unorganised conglomeratic channels (A2; Figure 2C) are composed of unsorted coarse sand to pebbles (F5; F6), with scarcely preserved fining upward trends (F7), humpback cross-beddings (F8; Figure 2F) (Fielding, 2006; Rust & Gibling, 1990) and planar laminations suggesting proximal upper flow regimes. Those occurrences are found beneath the Blanes and Viala amalgamated conglomerates (L2, L3, and L4) and within the Jonquières Formation (L6 and L7).

Isolated channels (A3; Figure 2B) show fining upward trends, large foresets, ripples to megaripples, and some pebble imbrications (F10; F11; Figure 2B; E), suggesting perennial currents (Hassan, 2005). Isolated channels are found from proximal to distal reaches with decreasing (i) grain size, (ii) channel dimensions, and (iii) frequency (Owen, Ebinghaus, et al., 2017). Upstream pebble-dominated channels are found within the Blanes Conglomerates and Flowers Formation (L2, L3, and L4), midstream sand-dominated channels are found within the Blanes Sandstones and Lacamp Formation (L2 and L8), and distal small sandy channels are described within the Lairière Silts (L9).

Floodplain facies associations

Crevasse splays (A4) are plane, fining upward, and laterally continuous sandstone sheets found adjacent to channels (F9). Present over the entire area, their frequency increases towards distal environments due to decreased channel confinement (Cain & Mountney, 2009; Owen, Ebinghaus, et al., 2017; Owen, Nichols, et al., 2017).

Paleosols (A5; Figure 2C) comprise clay to fine sandstones.

Rootlets, plant debris, mottling, and a possible columnar fabric inform on a calm, emerged paleosol (F1). Some hydromorphic paleosols are identified through various types of bioturbation and rare asymmetric ripples (F2). Paleosols are scarcely preserved in proximal reaches and abundant in medial (Blanes Sandstones, upper Flowers Formation, and Lacamp Formation) and distal areas (Lairière Silts).

Lacustrine facies associations

Lake deposits (A6; Figure 2F; G) comprise fine lithologies such as silts, fine sandstones, and carbonate mudstone to packstone. Plane laminations, intense bioturbation, numerous gastropods, plant debris, and algae (F2; F3) indicate calm and shallow environments. The laterally continuous lacustrine deposits of the Villerouge-Talairan Limestones (L1, L2, L3, and L4) are interpreted as relatively perennial lakes in distal areas (Benvenuti, 2003; Owen, Nichols, et al., 2017). In contrast, mud-dominated fine lake layers with limited lateral extension (F4) are found in medial reaches above channel lenses, which are interpreted as oxbow lakes.

Lacustrine deltas (A7) are defined by fining upward sand bodies with foresets (F10, sandy F11) within the Villerouge-Talairan lacustrine deposits (A6). It indicates that the lake developed at the distal mouth of a fluvial system.

Lacustrine turbidites (A8; Figure 2H) are pebble-dominated thin sheets spread through the Kiln lacustrine deposits (A6). Those coarse and unsorted deposits inform on gravity-driven processes.

4.2. Sequence stratigraphy

Facies trends are studied vertically, i.e., through time, from logs and outcrops. The Blanes outcrop reveals a transition from sand- to pebble-dominated isolated channels, with increasing

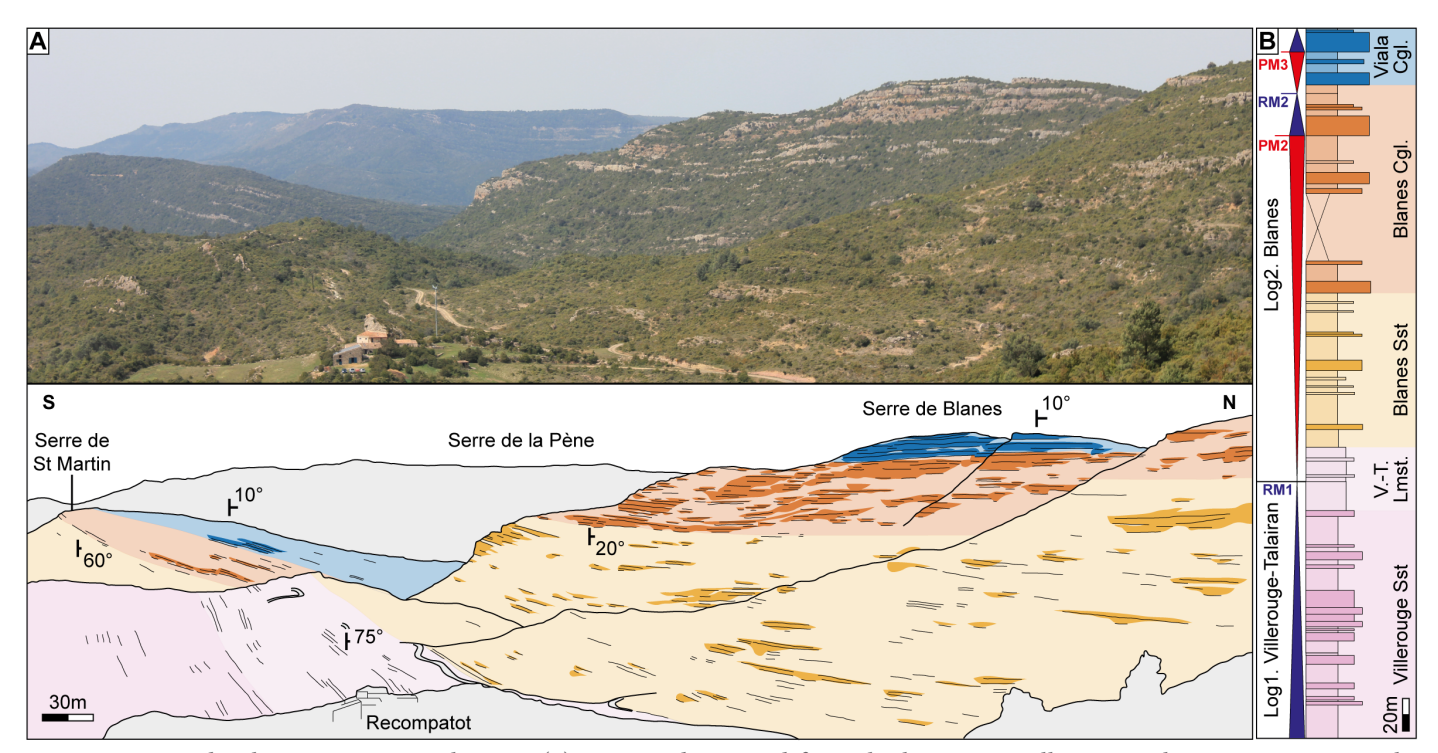


Figure 3: Serre de Blanes panorama, showing (1) a prograding trend from the lacustrine Villerouge-Talairan Limestone to the amalgamated Blanes and Viala Conglomerates and (2) syntectonic growth strata shown by a progressive up-section decrease in dips.

dimensions and frequency, until they become highly amalgamated on top of the section (Figure 3). The channel-fill coarsening and decreased floodplain preservation are interpreted as a prograding trend, with the progradation maximum (PM) located amongst the coarsest channels and the deposits of highest amalgamation.

Increasing abundance in floodplain facies through time, sometimes associated with interbedded lacustrine deposits, proves retrograding trends. This phenomenon is observed on a large scale with the Villerouge-Talairan Limestones, which outcrop in the east and are synchronous with the relatively thick Talairan Limestones (Crochet, 1991; Ellenberger et al., 1985). Retrogradation maxima (RM) are represented by lacustrine deposits when present. Otherwise, they are located within relatively thick alluvial plain deposits (Shanley & McCabe, 1991).

4.3. Geological mapping and correlation transect

Sequence stratigraphic concepts applied to the different logs within the Palassou First Unit in the Talairan Syncline show four successive sequences of progradation and retrogradation. The geological map (Figure 4) and the correlation transects (Figure 5) enable the identification of sediment thicknesses and lateral facies variations, as well as tectonic features. On a broad scale, sequences 1 to 3 are the thickest to the South of the Lagrasse Massif, along the Orbieu Valley (Figure 4). In contrast, Sequence 4 is solely preserved on the western side of the Talairan Syncline (Figure 4). The thickness variations from east to west appear to correspond to the north-40° oriented Mayronnes, Caunettes, and Hautes Jonquières faults, which are emplaced in the continuation of the Lagrasse thrust (Figure 4). The north-40° faults are strike-slip structures that displace the llerdian strata and only parts of the Palassou First Unit strata (Figure 4), suggesting active tectonics during the whole deposition of the Palassou First Unit. A detailed tectono-sedimentary description of each sequence is provided below.

Sequence 1

The first depositional sequence (shown in pink colors in Figures 4 and 5) is defined from the Villerouge-Talairan log (L1; Figure S2). The first deposits of the Palassou Formation, which overlie the Ilerdian deltas, consist of floodplain deposits with abundant

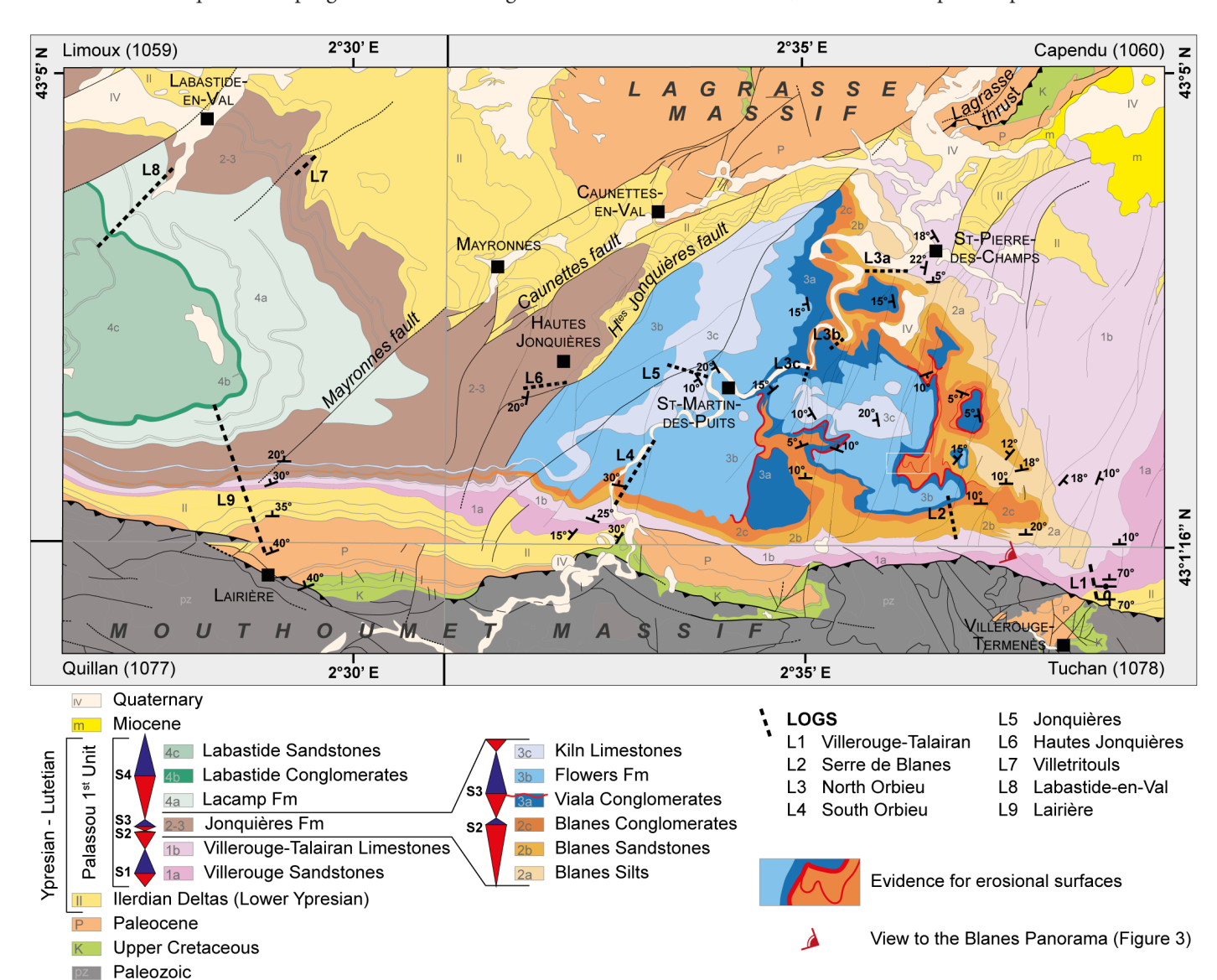


Figure 4: Detailed geological map of the Talairan Syncline. This study provides the details of the Palassou First Unit, based on the logs (dashed lines), and showing four stratigraphic sequences: sequence one (1a-1b) in pink, sequence two (2a-2c) in orange, sequence three (3a-3c) in blue, and sequence four (4a-4c) in green. Erosional surfaces are marked with red lines. Other formation limits are from published geological maps (Berger et al., 1997; Crochet et al., 1989; Ellenberger et al., 1985; Lenguin & Ovtracht, 1977).

crevasse splays and some sandy to conglomeratic isolated channels with NNW-oriented paleocurrents (Figure 7A). Grouped in the Villerouge Sandstones formation, the first progradation maximum (PM1) is identified within the coarsest channel, overlaid by extensive and well-formed paleosols. Overlying the Villerouge Sandstones are the Villerouge-Talairan Limestones, corresponding to lacustrine deposits (Crochet, 1991; Ellenberger et al., 1985) and comprising the first retrogradation maximum (RM1).

The deposits from Sequence 1 are thicker in the southeast of the Talairan Syncline, measuring 250m in the Villerouge-Talairan log (L1), 160m in the North Orbieu log (L3a), and 115m in Lairière (L9). This sequence is not precisely distinguished in the northeastern part of the basin, in the Villetritouls log (L7).

Analysed dips along the Villerouge-Talairan log, located at the

southern edge of the Talairan Syncline, show reversed Lower Ypresian deposits (south dipping of 70°) overlaid by vertical horizons of the Villerouge Sandstones and gently northward dipping (10°) lacustrine Villerouge-Talairan Limestones. The progressive dip variations illustrate a tectono-sedimentary wedge located just north of the Mouthoumet Front Thrust, which develops during the first sequence (Figure 3) (Christophoul et al., 2003).

Sequences 2 and 3

Sequence 2 (shown in orange colors in Figures 3 and 4), defined in the Blanes log (L2), comprises alluvial deposits. It is characterized by a clear progradation trend, from the Blanes Silts, which are dominated by paleosols and crevasse splay deposits, to the Blanes Sandstones, where NW-oriented, isolated channels become increasingly frequent and are mostly sandy, to

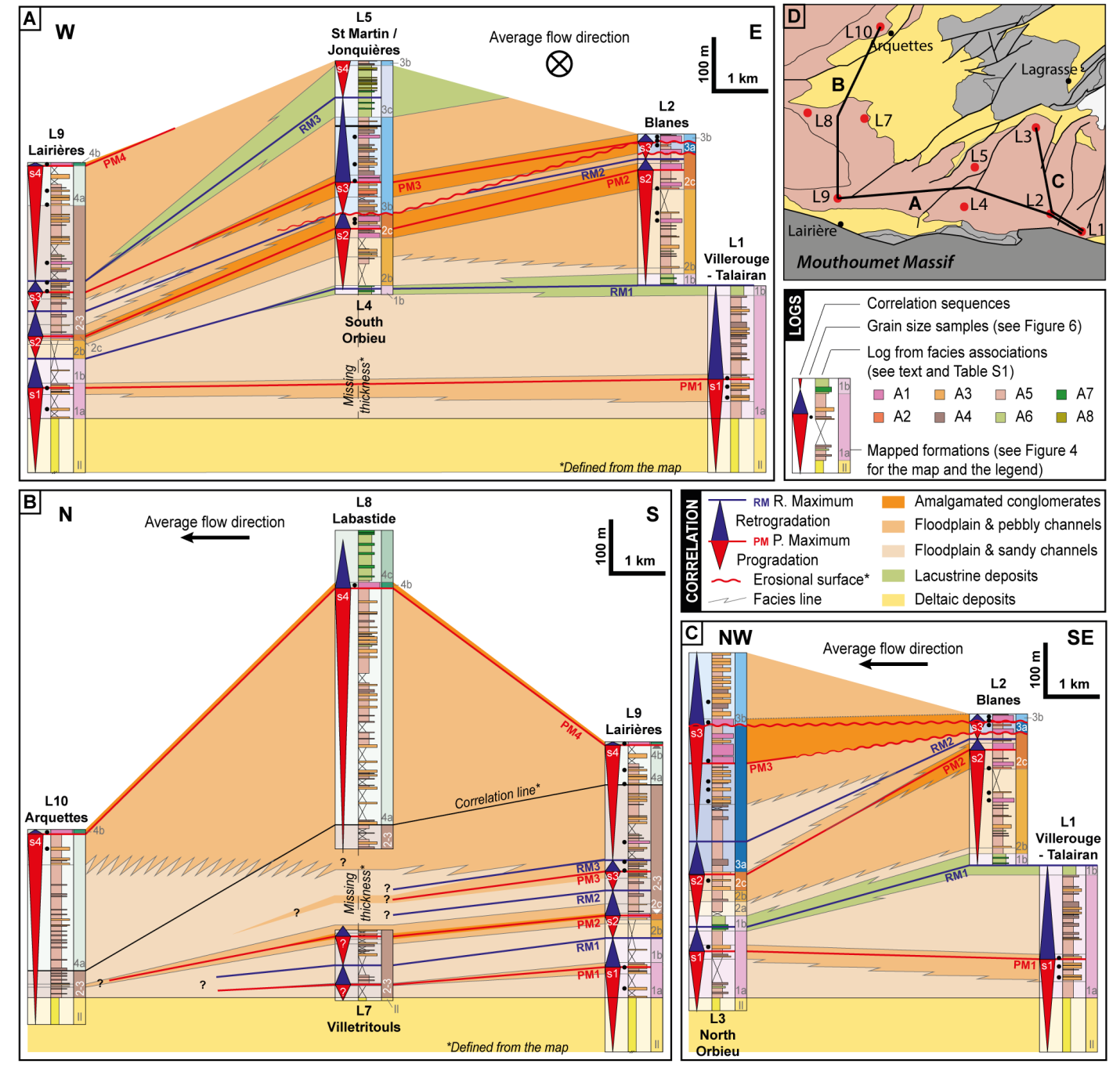


Figure 5: Correlation transect through the Talairan Syncline. (A) Westward thinning of sequences 1 to 3. (B) N-S thickness variations in the western part of the syncline, with Sequence 4 thickening north of the Lagrasse Massif. (C) N-S thickness variations in the eastern part of the syncline. (D) Location map of the logs and the transects (see Figure 1 for the references).

the Blanes Conglomerates, marked by amalgamated conglomeratic channels (Figure 3). A limited retrogradation is recorded in Sequence 2. Sequence 3 (shown in blue in Figures 3 and 4) comprises the amalgamated Viala Conglomerates, showing scattered paleocurrents to the northwest (Figure 7B) and constituting the third progradation maximum (PM3). The third retrogradation maximum (RM3) lies within the lacustrine Kiln Limestones intercalated within the fluvial Flowers Formation that shows a shift in paleocurrent direction towards the west (Figure S2; L4, L5).

The second and third sequences are 300m thick within the Talairan Syncline (Figure 5). West of the Hautes Jonquières fault, the first three sequences correspond to the Jonquières Formation (Figure 4), which is 100m thick near Villetritouls (L7) and 50m thick near Arquettes-en-Val (L10, Figure 1C).

Numerous erosional contacts are identified at the base of the Viala Conglomerates and Flowers Formation (Figures 4 and 5; Figure S1), corresponding to significant angular unconformities. They are the most erosive in the south, i.e., in the proximal margin of the basin. Moreover, the growth strata shown for Sequence 1 continue within Sequences 2 and 3 (Figure 3).

Sequence 4

Sequence 4 (in green in Figure 4) is defined from the Labastide-en-Val log (L8, Figure S2) and outcrops to the west of the Talairan Syncline. Most of the sequence comprises poorly developed paleosols with sandy to conglomeratic isolated channels containing some humpback cross-bedding (Figure 2E), defined by the Lacamp Formation. On top lies the 11-meter-thick amalgamated Labastide Conglomerate, with NNW-oriented paleocurrents and interpreted as the fourth progradation maximum

in the Talairan Syncline (PM4). The following retrogradation is recorded in the Labastide Sandstones, composed of well-developed paleosols, lacustrine intervals, and isolated conglomeratic channels.

Although the bulk deposits of the first three sequences are confined within the Talairan Syncline between the Mouthoumet Massif and Lagrasse Massif, the time line drawn at the base of the Lacamp Formation (Figure 4; Figure 5B) suggests the fourth progradation thickens northward from Lairière (30m) to Labastide-en-Val (490m) and then thins progressively toward Arquettes-en-Val (260m) (Figure 5B).

4.5. Grain size fining rates

Median and 84th percentile grain sizes are plotted against radial downstream distance (Figure 6), the apex of each sequence being located on the Mouthoumet Thrust (Figure 7). Progradation 1 shows a median input grain size of 14.9 \pm 0.9 mm and a fining rate of 0.09 ± 0.01 along a system length of 13 km (Figure 6A). The input D_{84} is 26.3 \pm 1.5 mm and shows a similar fining rate of 0.07 \pm 0.01. Sequence 2 shows coarser clasts, with an input D_{50} of 41.3 \pm 14.2 mm and an input D_{84} of 114.9 \pm 38.6 mm. The fining rates of the second sequence are 0.48 \pm 0.11 and 0.53 \pm 0.11 for the $D_{_{50}}$ and $D_{_{84}}\!,$ respectively, over a 5 km distance (Figure 6B). The grain sizes of Sequence 3 show intermediate values, with input D_{50} of 21.4 ± 3.9 mm and input D_{84} of 43.8 ± 6.7 mm. Fining rates are also relatively high, from $0.28 \pm$ 0.06 for $\rm D_{50}$ to 0.23 \pm 0.04 for $\rm D_{84}$ over 8 km (Figure 6C). Finally, grain sizes from Progradation 4 do not follow an exponential law with respect to downstream distance. The D_{50} and D_{84} remain constant throughout the system, with mean and standard deviation values of 7.3 \pm 0.9 mm and 14.2 \pm 2.5 mm, respectively (Figure 6D).

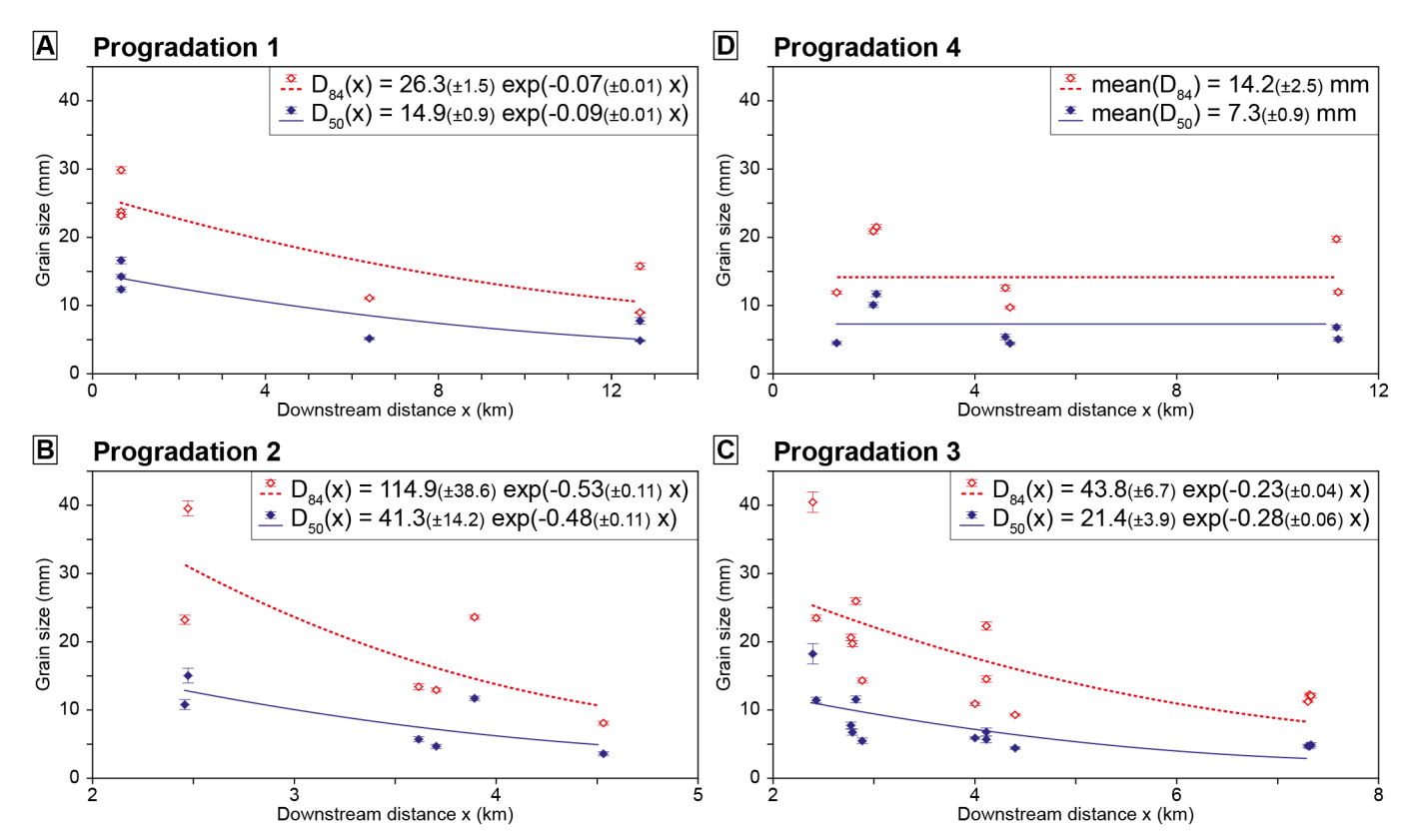


Figure 6: Grain size evolution with downstream distance for Progradation 1 (A), Progradation 2 (B), Progradation 3 (C), and Progradation 4 (D). D_{50} values are shown in blue, plain dots and plain lines, and D_{84} in red, empty dots and dashed lines. Lines are best-fit regressions, with the associated equations and uncertainties indicated.

5. Discussion

5.1. Sedimentary system

Various terrestrial facies have been identified within the Palassou First Unit in the Talairan Syncline, which helps create a more accurate depiction of the landscape at the time of its deposition.

Fluvial systems are defined from proximal to distal by (i) amalgamated conglomeratic channels, (ii) conglomeratic channels isolated in fine floodplain deposits, and (iii) sandy channels isolated in floodplain deposits with developed paleosols. Distal fluvial sections exhibit finer grain sizes and less frequent channels, indicating lower energy and well-developed paleosols, which suggests a lower sediment flux. These downsystem changes in facies could be linked with distributive fluvial systems (Owen, Nichols, et al., 2017), even though not all criteria are assessed (Fielding et al., 2012; Owen, Nichols, et al., 2017). In any case, alluvial facies indicate a downstream decrease in flow energy and multiple channels, rather than a single major fluvial channel, within the Palassou First Unit in the Talairan Syncline.

Lacustrine deposits are observed where sedimentation rate is the highest (Figure 5), suggesting a deposition driven by accommodation. The Villerouge-Talairan Limestones, deposited at Retrogradation Maximum 1, are characterized by very finegrained, limestone-dominated sediments. The Villerouge-Talairan Limestones cover most of the eastern Talairan Syncline (Crochet, 1991; Plaziat, 1981) and thins towards the west before Lairières (Figure 5B). The Kiln Limestones, deposited at Retrogradation Maximum 3, show an alternation of limestone and conglomerates. A westward shift in fluvial channel direction is observed in the upper part of the Flowers Formation (South Orbieu log, L4; Figure S2). The shift from transverse to axial drainage in the Talairan Syncline could have led to the deposition of the Kiln Limestone (Figure 7C). Because the Kiln Limestones deposit just before the bypass of the Talairan Syncline, we hypothesize that its deposition is tectonically driven by drainage reorganisation. This hypothesis is strengthened by the fact that the following deposits of Sequence 4 are characterized by a northwest-oriented dispersive system away from the Mayronnes fault (Figure 7D), which is similar to the prograding systems of Sequences 2 and 3.

5.2. Syn-tectonic basin filling

Following the Paleocene tectonic quiescence (Angrand & Mouthereau, 2021; Ford et al., 2022), the basal Eocene is characterized by the reactivation of the Pyrenean collision. Uplift of the North Pyrenean and Axial Zones (Ford et al., 2016; Ternois et al., 2019; Whitchurch et al., 2011) led to the creation of a flexural basin between the active Mouthoumet Thrust, a subunit of the North Pyrenean Frontal Thrust, and the Montagne Noire peripheral relief. In the Corbières area, the first stage of basin development is recorded in the middle Ypresian Palassou Formation (Early Cuisian), with syn-tectonic growth strata primarily identified on geological maps (Berger et al., 1997; Christophoul et al., 2003; Martín-Martín et al., 2001). This study offers a deeper understanding of the interplay between tectonics and sedimentation in the early stages of the Pyrenean retro-foreland's flexure.

Sequences 1 and 2 are characterized by progressive dip varia-

tions, as illustrated by growth strata at the front of the Mouthoumet Massif frontal thrust (Figure 3), which are represented in the Tuchan geological map (Berger et al., 1997). Moreover, sequences 1 and 2 thin from the Mouthoumet Thrust in Villerouge-Talairan and Blanes towards the north of the Orbieu Valley (Figure 5C). Sequences 2 and 3 show internal erosional angular truncation surfaces (Figure 4; Figure S1). Growth strata, thickness variations, and erosional surfaces mark a syn-depositional flexure of the basin (DeCelles & Giles, 1996) in the early stages of the deposition of the Palassou First Unit. Sequences 1 to 3 pinch out on the active Lagrasse Massif, which wasn't active during the Lower Ypresian, when the Ilerdian delta crossed over this massif (Christophoul et al., 2003). Beyond these down-dip trends, substantial along-strike variations occur at the front of the Mouthoumet thrust. Sequences 1 to 3 thin towards Lairières in the West (Figure 5B), showing a less subsident area and a non-cylindrical depocenter at the Mouthoumet Thrust Front. Our data show that the westward thinning is bounded by the NE-SW-oriented Mayronnes, Caunettes, and Hautes Jonquières oblique faults (Figure 4). These NE-SW structures are widely distributed over the Talairan Syncline and affect the Palassou First Unit, although our detailed mapping evidence a syn-depositional activity of these faults. This oblique structure set seems to extend and connect to the Lagrasse Thrust (Figure 4), to which they seem kinetically compatible, given the strike-slip motion along the NE-SW fault and the north-east direction of the thrusting. Parizot et al. (2021) obtained a Lutetian age (43.2 \pm 5.3 Ma) using U/Pb dating on syn-kinematic calcite in the Cagalière duplex (CD in Figure 1), related to the Lagrasse structure. A Lutetian activity of the Lagrasse structure is congruent with our observed sedimentary record, especially when considering the multiphase tectonic history of this structure (Souque et al., 2003), and the possibly more ancient age (48.7 \pm 2 Ma) obtained from contractional slickenfibers just to the north (Parizot et al., 2021). At the western termination of the Mouthoumet Thrust, near Limoux (Figure 1), growth strata within the Palassou First Unit are sealed by the Bartonian strata of the Palassou Second Unit (Crochet, 1991; Crochet et al., 1989). In conclusion, the syn-tectonic system of the Palassou First Unit is characterized by a non-homogeneous distribution of subsidence from east to west, suggesting that lateral variations in shortening and deformation are bounded by NE-SW faults that accompany the progressive fading of the Mouthoumet Thrust to the west.

5.3. Large-scale progradation

The Palassou First Unit deposits show a general large-scale progradation of sediments, marked by the northward migration of the depocenter from sequences 1 to 4 in the studied area. Sequences 1 and 2 are the thickest at the Mouthoumet Front (Figure 5C). In contrast, the depocenter of Sequence 3 is in the center of the Talairan Syncline (Figure 5C), and that of Sequence 4 is shifted to the north-west of the Mayronnes fault (Figure 5B). In terms of facies, the progradation maxima of PM2 and PM3 are similar, characterized by amalgamated conglomerates on the southern edge of the basin. However, PM2 shows a rapid facies variation towards isolated channels, whereas PM3 progrades further north and exhibits more internal erosional surfaces (Figure 5C). This outward shift could be due to the progradation of Sequence 3 over the deposits of Sequence 2, with further sediment export towards the toe of the previous system, where accommodation is higher. Yet, both sequences 2 and 3 are marked by syn-tectonic deposition. Therefore, we can

hypothesize that subsidence impacts these sequences and that the folding and thrusting in the Lagrasse Massif may have mitigated the northward progradation of the sedimentary systems. Still, the study of geometries and facies variations highlights a distribution of facies dictated by the morphology of the deposits and the global prograding trend. Sequence 4 evidences a large-scale progradation of the gravel front over these different structures (Figure 7D), suggesting a dominance of sediment supply over the subsidence rate and inherited topography.

At the regional scale of the eastern retro-foreland during Upper Ypresian (Cuisian) and Lutetian (Figure 7E), the export of sediments from the Montagne Noire is limited to the northern fringe (Figure 7E) (Chaigne, 1964; Plaziat, 1981), making the Pyrenees the major source area of the Corbières Basin. Two stages are identified within the Cuisian-Lutetian period. During the first stages of the continental fill (Sequences 1 to 3 in this study), coarse sediments are trapped within the Talairan and Chalabre synclines (Figure 7E) (this study; Crochet, 1991), and

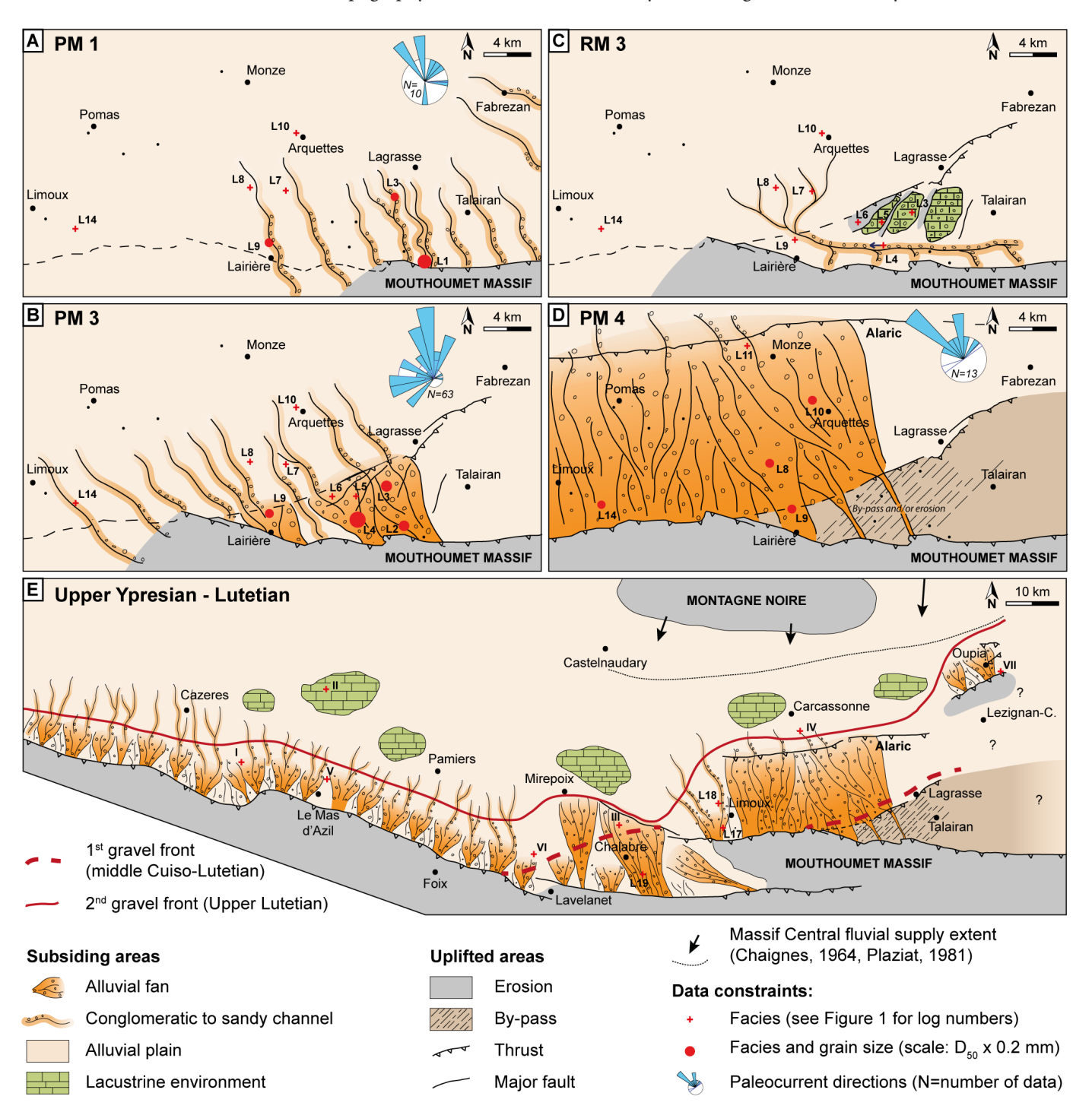


Figure 7: Paleogeography of the Talairan Syncline and north-east retro foreland basin during the deposition of the Palassou First Unit. (A) Progradation Maximum 1: in the Talairan syncline, small-sized fluvial systems flow to the north-west, fed by the Mouthoumet Massif. (B) Progradation Maximum 3: the Mouthoumet Thrust extends to the west, and the activated Lagrasse and Mayronnes fault system traps coarse sediments in the Talairan Syncline. (C) Retrogradation Maximum 3: paleocurrents shift to the west, and lacustrine deposits with coarse sediment input lie in the northern edge of the Talairan Syncline. (D) Progradation Maximum 4: the Talairan Syncline is overfilled, and sedimentation shifts to the west, between the Lagrasse and Alaric structures. (E) Palassou First Unit at the regional scale: deposits from sequences 1 to 3 are limited to the Talairan Syncline and the Chalabre Basin, as shown by the first gravel front (dashed red lines). Sequence 4 expresses the maximum progradation of the gravel front over the entire eastern retro-foreland (continuous red line) within the Palassou First Unit.

a first gravel front is defined at the Lagrasse and Mirepoix structures (dashed red lines in Figure 7E). The large-scale progradation occurs during the second stage (starting from Sequence 4 in the Talairan Syncline), leading to a northward shift of the depocenters and the gravel front to the Alaric structure (Figure 7D; E) and the Oupia systems in the north-east (Figure 7E) (Mauduit, 1981).

5.4. Controlling factors: Subsidence versus flux

Progradation maxima have different patterns in terms of downstream grain size fining (Figure 6) and facies transitions (Figure 5). The fining rate of Sequence 1 is relatively low and compares with the fining rates of sequences marked by limited subsidence in other studies (Figure 6A) (D'Arcy et al., 2016; Duller et al., 2010; Reynolds, 2024; Whittaker et al., 2011). However, Sequence 1 is clearly marked by growth strata, shown from the dip variations in the Villerouge-Talairan log (L1) and on the Blanes panorama (Figure 3). It is therefore surprising to have a relatively low fining rate. On the other side, sedimentary flux also increased drastically during Sequence 1, as shown by the shift from a deltaic to an alluvial depositional environment with coarse-grained channel-fills (PM1). Because the fining rate results from the interplay between subsidence and flux (Armitage et al., 2011; Robinson & Slingerland, 1998; Whittaker et al., 2011), we hypothesize that Sequence 1 was influenced by both high subsidence and high sedimentary fluxes, with these two factors being relatively balanced.

The significant increase in fining rate at Sequences 2 and 3, combined with a slight increase in the input grain size (Figure 6B; C), suggests subsidence-driven progradations (Armitage et al., 2011; Duller et al., 2010; Whittaker et al., 2011). This analytical interpretation is entirely consistent with the abundance of syn-tectonic features observed within the deposits of these three sequences, namely the growth strata and successive erosional truncations (Figures 4 and 5). Tectonics, through the first stages of the retro-foreland flexure, is therefore the main factor controlling sedimentation at the foothill of the Pyrenees.

In contrast, Sequence 4 shows no downstream fining, coupled with a net increase in the downstream length of the coarse-deposits fluvial system (Figure 6D; Figure 7D). The system lengthening and absence of grain size fining indicate a rise in transport capacity, interpreted as a flux-driven progradation (Armitage et al., 2011; D'Arcy et al., 2016; Paola et al., 1992). Increased flux from the catchment can be induced by an increase in rainfall or catchment area (Li et al., 2021; Syvitski & Milliman, 2007; Whipple & Tucker, 1999). Boyrie et al. (2025) suggest that monsoon-type hydrological regimes prevailed during the EECO in the nearby Minervois Basin, based on sedimentological analysis and temperature changes in the subtropical paleolatitude of the area. A similar process could explain the progradations observed in the Corbières area at the EECO; however, more accurate dating and chemostratigraphy data are needed to test this hypothesis. An increase in drainage area during the deposition of the Palassou First Unit at the time of increasing shortening in the orogen is highly plausible. Indeed, Crochet (1991) identified a change in clast composition from Mesozoic and Cenozoic cover clasts and Paleozoic ones locally sourced from the Mouthoumet Massif within the First Palassou Unit, to Paleozoic sedimentary and plutonic rocks within the Second Unit. The arrival of granitic clasts indicates a change in source area, first eroding the Mouthoumet Massif cover coevally to the Palassou First Unit, and then reaching the exhumed North Pyrenean and Axial Zone granitic massifs during the deposition of the Palassou Second Unit (Crochet, 1991). A more precise provenance analysis conducted on the different sequences of the Palassou First Unit will help determine whether the enlargement of the source area occurred progressively and could explain the observed large-scale progradation.

Another result of this study is the congruence between (1) the syn-sedimentary tectonics, evidenced from detailed mapped geometries, correlation transects, and the evolution through time of the depocenter location, and (2) the fining rates obtained for each sequence. As such, this study constitutes an indirect validation of the grain-size fining methodology. At the scale of the entire sediment routing system, this study suggests that, in the initial stages of orogenic growth, the sediment supply is confined within the frontal basin and fold-and-thrust belts due to dominant subsidence. In contrast, Qs dominates in a second stage, leading to massive export of sediments to the foreland basin.

6. Conclusions

This study presents a detailed stratigraphy of the Lower Eocene continental molasse in the Pyrenean retro-foreland, questioning the relative importance of subsidence and flux in shaping the architecture and lithology of the basin fill during the initial stages of the flexure. Facies analyses, mapping, and sequence stratigraphy applied to the Palassou First Unit in the Talairan Syncline led to the identification of four depositional sequences. Each sequence exhibits clear tectonic features, indicating a strong tectonic influence on sedimentation. High grain size downstream fining rates confirm high subsidence during the first three sequences. At this stage, coarse sediments were trapped within the Talairan Syncline. The fourth sequence corresponds to a regional progradation of the gravel front towards the north-west. This progradation, associated with a doubling of the export distance of coarse sediments and an absence of grain size fining, marks a stage of enhanced flux. This study establishes the tectono-stratigraphic scheme of the Pyrenean retro-foreland at the onset of the major tectonic pulse, illustrating various infill stages influenced by tectonic structures and the evolution of sedimentary and water fluxes over time. These data pave the way for more accurate deciphering of how provenance evolved over time and how the EECO impacted these tectonically active catchments.

Acknowledgement

This work was funded and carried out within the framework of the BRGM-TOTAL Source-to-Sink project. The authors are thankful to Thomas Dewez for valuable help in photogrammetry, to Chantal Bourdillon ERADATA for specific foraminifera dating, and to Laurence and Alain Bruet for their warm welcome during field missions. We are grateful to Nicolas Loget, Sylvain Calassou, and Charlotte Fillon for their constant support and constructive discussions, and to Cécile Allanic for her valuable advice on structural aspects.

Authors contribution

Marine Prieur, Justine Briais, and Eric Lasseur participated in the project's conceptualization and methodology, in the field work and data collection, and in the writing and editing of the manuscript. Eric Lasseur and Justine Briais led supervision. Eric Lasseur proposed the project and applied for S2S funding.

Data availability statement

All data are presented in the article and in the Supplementary Materials.

Conflict of interest

The authors declare no conflict of interest.

References

Al Reda, S. M., Barbarand, J., Gautheron, C., Lasseur, E., Loget, N., Pinna-Jamme, R., & Briais, J. (2021). Thermal record of the building of an orogen in the retro-foreland basin: Insight from basement and detrital thermochronology in the eastern Pyrenees and the north Pyrenean basin (France). Basin Research, 33(5), 2763-2791. https://doi.org/10.1111/bre.12583

Allen, P. A. (1981). Sediments and processes on a small stream-flow dominated, Devonian alluvial fan, Shetland Islands. Sedimentary Geology, 29, 31-66. https://doi.org/0037-0738/81/0000--0000/\$02.50

Allen, P. A., Armitage, J. J., Carter, A., Duller, R. A., Michael, N. A., Sinclair, H. D., Whitchurch, A. L., Whittaker, A. C., & Schlunegger, F. (2013). The Qs problem: Sediment volumetric balance of proximal foreland basin systems. Sedimentology, 60(1), 102-130. https://doi.org/10.1111/sed.12015

Angrand, P., & Mouthereau, F. (2021). Evolution of the Alpine orogenic belts in the Western Mediterranean region as resolved by the kinematics of the Europe-Africa diffuse plate boundary. BSGF - Earth Sciences Bulletin, 192. https://doi.org/10.1051/bsgf/2021031

Armitage, J. J., Duller, R. A., Whittaker, A. C., & Allen, P. A. (2011). Transformation of tectonic and climatic signals from source to sedimentary archive. Nature Geoscience, 4(4), 231-235. https://doi.org/10.1038/ngeo1087

Averbuch, O., Frizon de Lamotte, D., & Kissel, C. (1992). Magnetic fabric as a structural indicator of the deformation path within a fold-thrust structure: a test case from the Corbières (NE Pyrenees, France). Journal of Structural Geology, 14(4), 461-474. https://doi.org/10.1016/0191-8141(92)90106-7

Baby, P., Crouzet, G., Specht, M., Deramond, J., Bilotte, M., & Debroas, E. J. (1988). Rôle des paléostructures albo-cénomaniennes dans la géométrie des chevauchements frontaux nord-pyrénéens. C. R. Acad. Sci. Paris, 306, 307-313.

Beaumont, C., Muñoz, J. A., Hamilton, J., & Fullsack, P. (2000). Factors controlling the Alpine evolution of the central Pyrenees inferred from a comparison of observations and geodynamical models. Journal of Geophysical Research: Solid Earth, 105(B4), 8121-8145. https://doi.org/10.1029/1999jb900390

Benvenuti, M. (2003). Facies analysis and tectonic significance of lacustrine fan-deltaic successions in the Pliocene–Pleistocene Mugello Basin, Central Italy. Sedimentary Geology, 157(3-4), 197-234. https://doi.org/10.1016/s0037-0738(02)00234-8

Berger, G., Bessière, G., Bilotte, M., & Viallard, P. (1997). Carte géologique de la France à 1/50000 - Feuille 1078 - Tuchan. Bureau de Recherches Géologiques et Minières,

Boyrie, C., Girard, F., Yans, J., Ballas, G., Lihoreau, F., Benammi, M., Bourget, H., Garcia, G., Leredde, C., Pellissier-Tanon, A., Valentin, X., Vidalenc, D., & Tabuce, R. (2025). Abrupt changes in continental sedimentation triggered by monsoon-type event during EECO hyperthermals, Minervois Basin, Southern France. Sedimentary Geology, 486. https://doi.org/10.1016/j.sedgeo.2025.106923

Cain, S. A., & Mountney, N. P. (2009). Spatial and temporal evolution of a terminal fluvial fan system: the Permian Organ Rock Formation, South-east Utah, USA. Sedimentology, 56(6), 1774-1800. https://doi.org/10.1111/j.1365-3091.2009.01057.x

Chaigne, M. (1964). Contribution à l'étude stratigraphique et sédimentologique du secteur Aigne-Tourouzelle. Bassin Tertiaire de Carcassonne. In F. d. S. d. l. U. d. Bordeaux (Ed.).

Christophoul, F., Soula, J. C., Brusset, S., Elibana, B., Roddaz, M., Bessiere, G., & Deramond, J. (2003). Time, place and mode of propagation of foreland basin systems as recorded by the sedimentary fill: examples of the Late Cretaceous and Eocene retro-foreland basins of the north-eastern Pyrenees. Geological Society, London, Special Publications, 208(1), 229-252. https://doi.org/10.1144/gsl.Sp.2003.208.01.11

Cramer, B. S., Toggweiler, J. R., Wright, J. D., Katz, M. E., & Miller, K. G. (2009). Ocean overturning since the Late Cretaceous: Inferences from a new benthic foraminiferal isotope compilation. Paleoceanography, 24(4). https://doi.org/10.1029/2008pa001683

Crochet, B. (1991). Molasses syntectoniques du versant nord des Pyrénées : La série de Palassou BRGM.

Crochet, B., Villatte, J., Tambareau, Y., Bilotte, M., Bousquet, J.-P., Kuhfuss, A., Bouillin, J.-P., Gélard, J.-P., Bessiere, G., & Paris, J.-P. (1989). Carte géologique de la France à 1/50000 - Feuille 1077 - Quillan. Bureau de Recherches Géologiques et Minières,

D'Arcy, M., Whittaker, A. C., Roda-Boluda, D. C., & Bristow, C. (2016). Measuring alluvial fan sensitivity to past climate changes using a self-similarity approach to grain-size fining, Death Valley, California. Sedimentology, 64(2), 388-424. https://doi.org/10.1111/sed.12308

DeCelles, P. G., & Giles, K. A. (1996). Foreland basin systems. Basin Research, 8, 105-123. https://doi.org/https://doi.org/10.1046/j.1365-2117.1996.01491.x

Duller, R. A., Whittaker, A. C., Fedele, J. J., Whitchurch, A. L., Springett, J., Smithells, R., Fordyce, S., & Allen, P. A. (2010). From grain size to tectonics. Journal of Geophysical Research: Earth Surface, 115(F3). https://doi.org/10.1029/2009jf001495

Durand-Delga, M., & Charrière, A. (2012). Tectonique tangentielle fini-crétacée au front NE du massif de Mouthoumet (Pinède de Durban - Serre de Ginoufré, Corbières, Aude). Géologie de la France, 2, 25-48.

El Garouani, A., Alobeid, A., & El Garouani, S. (2014). Digital surface model based on aerial image stereo pairs for 3D building. International Journal of Sustainable Built Environment,

3(1), 119-126. https://doi.org/10.1016/j.ijsbe.2014.06.004

Ellenberger, F., Plaziat, J.-C., Freytet, P., Jaffrézo, M., Charrière, A., l'Homer, A., Legrand-Lespinasse, N., Huguet, J., Bessière, G., & Berger, G. (1985). Carte Géologique de la France à 1/50000 - Feuille 1060 - Capendu. Bureau de Recherches Géologiques et Minières,

Fedele, J. J., & Paola, C. (2007). Similarity solutions for fluvial sediment fining by selective deposition. Journal of Geophysical Research: Earth Surface, 112(F2). https://doi.org/10.1029/2005jf000409

Fielding, C. R. (2006). Upper flow regime sheets, lenses and scour fills: Extending the range of architectural elements for fluvial sediment bodies. Sedimentary Geology, 190(1-4), 227-240. https://doi.org/10.1016/j.sedgeo.2006.05.009

Fielding, C. R., Ashworth, P. J., Best, J. L., Prokocki, E. W., & Smith, G. H. S. (2012). Tributary, distributary and other fluvial patterns: What really represents the norm in the continental rock record? Sedimentary Geology, 261-262, 15-32. https://doi.org/10.1016/j.sedgeo.2012.03.004

Ford, M., Hemmer, L., Vacherat, A., Gallagher, K., & Christophoul, F. (2016). Retro-wedge foreland basin evolution along the ECORS line, eastern Pyrenees, France. Journal of the Geological Society, 173(3), 419-437. https://doi.org/10.1144/jgs2015-129

Ford, M., Masini, E., Vergés, J., Pik, R., Ternois, S., Léger, J., Dielforder, A., Frasca, G., Grool, A., Vinciguerra, C., Bernard, T., Angrand, P., Crémades, A., Manatschal, G., Chevrot, S., Jolivet, L., Mouthereau, F., Thinon, I., Calassou, S. (2022). Evolution of a low convergence collisional orogen: a review of Pyrenean orogenesis. BSGF - Earth Sciences Bulletin, 193. https://doi.org/10.1051/bsgf/2022018

Garefalakis, P., do Prado, A. H., Mair, D., Douillet, G. A., Nyffenegger, F., & Schlunegger, F. (2023). Comparison of three grain size measuring methods applied to coarse-grained gravel deposits. Sedimentary Geology, 446. https://doi.org/10.1016/j.sedgeo.2023.106340

Greenwood, D. R., & Wing, S. L. (1995). Eocene continental climates and latitudinal temperature gradients. Geology, 23(11), 1044-1048.

Hartley, A. J., Owen, A., Swan, A., Weissmann, G. S., Holzweber, B. I., Howell, J., Nichols, G., & Scuderi, L. (2015). Recognition and importance of amalgamated sandy meander belts in the continental rock record. Geology, 43(8), 679-682. https://doi.org/10.1130/g36743.1

Hassan, M. A. (2005). Characteristics of Gravel Bars in Ephemeral Streams. Journal of Sedimentary Research, 75(1), 29-42. https://doi.org/10.2110/jsr.2005.004

Hoey, T. B., & Bluck, B. J. (1999). Identifying the controls over downstream fining of river gravels. Journal of Sedimentary Research, 69(1), 40-50. https://doi.org/1073-130X/99/069-40/\$03.00

Honegger, L., Adatte, T., Spangenberg, J. E., Rugenstein, J. K. C., Poyatos-Moré, M., Puigdefàbregas, C., Chanvry, E., Clark, J., Fildani, A., Verrechia, E., Kouzmanov, K., Harlaux, M., & Castelltort, S. (2020). Alluvial record of an early Eocene hyperthermal within the Castissent Formation, the Pyrenees, Spain. Climate of the Past, 16(1), 227-243. https://doi.org/10.5194/cp-16-227-2020

Lauretano, V., Hilgen, F. J., Zachos, J. C., & Lourens, L. J. (2016). Astronomically tuned age model for the early Eocene carbon isotope events: A new high-resolution d13Cbenthic record of ODP Site 1263 between \sim 49 and \sim 54 Ma. Newsletters on Stratigraphy, 49(2), 383-400. https://doi.org/10.1127/nos/2016/0077

Lauretano, V., Littler, K., Polling, M., Zachos, J. C., & Lourens, L. J. (2015). Frequency, magnitude and character of hyperthermal events at the onset of the Early Eocene Climatic Optimum. Climate of the Past, 11(10), 1313-1324. https://doi.org/10.5194/cp-11-1313-2015

Lenguin, M., & Ovtracht, A. (1977). Carte géologique de la France à 1/50000 - Feuille 1059 - Limoux. Bureau de Recherches Géologiques et Minières,

Li, D., Lu, X., Overeem, I., Walling, D. E., Syvitski, J., Kettner, A. J., Bookhagen, B., Zhou, Y., & Zhang, T. (2021). Exceptional increases in fluvial sediment fluxes in a warmer and wetter High Mountain Asia. Science, 374(6567), 599-603. https://doi.org/10.1126/science.abi9649

Luciani, V., Dickens, G. R., Backman, J., Fornaciari, E., Giusberti, L., Agnini, C., & D'Onofrio, R. (2016). Major perturbations in the global carbon cycle and photosymbiont-bearing planktic foraminifera during the early Eocene. Climate of the Past, 12(4), 981-1007. https://doi.org/10.5194/cp-12-981-2016

Martín-Martín, M., Rey, J., Alcala-Garcia, F. J., Tosquella, J., Deramond, J., Lara-Corona, E., Duranthon, F., & Antoine, P.O. (2001). Tectonic controls on the deposits of a foreland basin: an example from the Eocene Corbières-Minervois basin, France. Basin Research, 13, 419-433. https://doi.org/https://doi.org/10.1046/j.0950-091x.2001.00158.x

Mauduit, E.-Y. (1981). Les unités pré-pyrénéennes du couloir de Carcassonne. Ensembles sédimentaires et structures. In U. P. S. d. Toulouse (Ed.).

Maufrangeas, A., Leleu, S., Loisy, C., Roperch, P., Jolley, D., Vinciguerra, C., & Nguyen-Thuyet, O. (2020). Stratigraphy of the Paleocene continental sedimentary succession of the northern Pyrenean basin (Corbières, southern France) using d13Corg isotopes. Journal of the Geological Society, 177(4), 752-765. https://doi.org/10.1144/jgs2019-084

McLeod, J. S., Whittaker, A. C., Hampson, G. J., Bell, R. E., Prieur, M., Fuller-Field, O. G., Valero, L., Yan, X., & Valenza, J. M. (2025). Hothouse Hydrology: Evolving River Dynamics in the Eocene Montllobat and Castissent Formations, Southern Pyrenees. Basin Research, 37(5). https://doi.org/10.1111/bre.70059

Olsen, T., Steel, R. J., Høgseth, K., Skar, T., & Røe, S.-L. (1995). Sequential architecture in a fluvial succession: Sequence stratigraphy in the Upper Cretaceous Mesaverde Group, Price Canyon, Utah. Journal of Sedimentary Research, B65(2), 265-281. https://doi.org/1073-1318/95/0B65-265/\$03.0C

Owen, A., Ebinghaus, A., Hartley, A. J., Santos, M. G. M., Weissmann, G. S., & Mountney, N. (2017). Multi-scale classification of fluvial architecture: An example from the Palaeocene–Eocene Bighorn Basin, Wyoming. Sedimentology, 64(6), 1572-1596. https://doi.org/10.1111/sed.12364

Owen, A., Nichols, G. J., Hartley, A. J., & Weissmann, G. S. (2017). Vertical trends within the prograding Salt Wash distributive fluvial system, SW United States. Basin Research, 29(1), 64-80. https://doi.org/10.1111/bre.12165

Paola, C., Heller, P. L., & Angevine, C. L. (1992). The large-scale dynamics of grain-size variation in alluvial basins, 1: Theory. Basin Research, 4(2), 73-90. https://doi.org/https://doi.org/10.1111/j.1365-2117.1992.tb00145.x

Parizot, O., Missenard, Y., Haurine, F., Blaise, T., Barbarand, J., Benedicto, A., & Sarda, P. (2021). When did the Pyrenean shortening end? Insight from U–Pb geochronology of syn-faulting calcite (Corbières area, France). Terra Nova, 33(6), 551-559. https://doi.org/10.1111/ter.12547

Pearson, P. N., Ditchfield, P. W., Singano, J., Harcourt-Brown, K. G., Nicholas, C. J., Olsson, R. K., Shackleton, N. J., & Hall, M. A. (2001). Warm tropical sea surface temperatures in the Late Cretaceous and Eocene epochs. Nature, 413, 481-470. https://doi.org/10.1038/35097000

Plaziat, J.-C. (1981). Late Cretaceous to Late Eocene palaeogeographic evolution of southwest Europe. Palaeogeography, Palaeoclimatology, Palaeoecology, 36, 263-320. https://doi.org/https://doi.org/10.1016/0031-0182(81)90110-3

Remondino, F., & El-Hakim, S. (2006). Image-based 3D modelling: A review. The Photogrammetric Record, 21(115), 269-291. https://doi.org/https://doi.org/10.1111/j.1477-9730.2006.00383.x

Reynolds, T. (2024). Grain size from source to sink – modern and ancient fining rates. Earth-Science Reviews, 250. https://doi.org/10.1016/j.earscirev.2024.104699

Robinson, R. A. J., & Slingerland, R. (1998). Origin of fluvial grain-size trends in a foreland basin: The Pocono Formation on the Central Appalachian Basin. Journal of Sedimentary Geology, 68(3), 473-486. https://doi.org/https://doi.org/10.2110/jsr.68.473

Romans, B. W., Castelltort, S., Covault, J. A., Fildani, A., & Walsh, J. P. (2016). Environmental signal propagation in sedimentary systems across timescales. Earth-Science Reviews, 153, 7-29. https://doi.org/10.1016/j.earscirev.2015.07.012

Rosenbaum, G., Lister, G. S., & Duboz, C. (2002). Relative motions of Africa, Iberia and Europe during the Alpine orogeny. Tectonophysics, 359, 117-129. https://doi.org/10.1016/S0040-1951(02)00442-0

Roure, F., Choukroune, P., Berastegui, X., Muñoz, J. A., Villien, A., Matheron, P., Bareyt, M., Seguret, M., Camara, P., & Deramond, J. (1989). ECORS deep seismic data and balanced cross sections: Geometric constraints on the evolution of the Pyrenees. Tectonics, 8(1), 41-50. https://doi.org/https://doi.org/10.1029/TC008i001p00041

Rust, B. R., & Gibling, M. R. (1990). Three-dimensional antidunes as HCS mimics in a fluvial sandstone: The Pennsylvanian South Bar Formation near Sydney, Nova Scotia. Journal of Sedimentary Petrology, 60(4), 540-548. https://doi.org/0022-4472/90/0060-540/\$03.00

Shanley, K. W., & McCabe, P. J. (1991). Predicting facies architecture through sequence stratigraphy - An example from the Kaiparowits Plateau, Utah. Geology, 19, 742-745. https://doi.org/https://doi.org/10.1130/0091-7613(1991)019<0742:P-FATSS>2.3.CO;2

Shanley, K. W., & McCabe, P. J. (1994). Perspectives on the Sequence Stratigraphy of Continental Strata. AAPG Bulletin, 78(4), 544-568. https://doi.org/https://doi.org/10.1306/BDFF9258-1718-11D7-8645000102C1865D

Shanley, K. W., McCabe, P. J., & Hettinger, R. D. (1992). Tidal influence in Cretaceous fluvial strata from Utah, USA: a key to sequence stratigraphic interpretation. Sedimentology, 39, 905-930. https://doi.org/https://doi.org/10.1111/j.1365-3091.1992. tb02159.x

Simpson, G., & Castelltort, S. (2012). Model shows that rivers transmit high-frequency climate cycles to the sedimentary record. Geology, 40(12), 1131-1134. https://doi.org/10.1130/g33451.1

Sinclair, H. D., & Naylor, M. (2012). Foreland basin subsidence driven by topographic growth versus plate subduction. Geological Society of America Bulletin, 124(3-4), 368-379. https://doi.org/10.1130/b30383.1

Souque, C., Frizon de Lamotte, D., Leturmy, P., & Robion, P. (2003). Duplex at the lateral tip of a thrust fault: the "La Cagalière" example (NE Pyrenees, France). Geodinamica Acta, 16(2-6), 89-98. https://doi.org/10.1016/s0985-3111(03)00004-4

Steel, R. J., & Ryseth, A. (1990). The Triassic - early Jurassic succession in the northern North Sea: megasequence stratigraphy and intra-Triassic tectonics. In R. F. P. Hardman & J. Brooks (Eds.), Tectonic Events Responsible for Britain's Oil and Gas Reserves (Vol. 55, pp. 139-168). Geological Society Special Publication. https://doi.org/https://doi.org/10.1144/GSL. SP.1990.055.01.07

Storz-Peretz, Y., & Laronne, J. B. (2013). Automatic Grain Sizing of vertical exposures of gravelly deposits. Sedimentary Geology, 294, 13-26. https://doi.org/10.1016/j.sedgeo.2013.05.004

Syvitski, J. P., & Milliman, J. D. (2007). Geology, geography, and humans battle for dominance over the delivery of fluvial sediment to the coastal ocean. Journal of Geology, 115, 1-19. https://doi.org/https://doi.org/10.1086/509246

Tambareau, Y., Crochet, B., Villatte, J., & Deramond, J. (1995). Evolution tectono-sédimentaire du versant nord des Pyrénées centre-orientales au Paléocène et à l'Eocène inférieur. Bull. Soc. géol. France, 166(4), 375-387. https://doi.org/https://doi.org/10.2113/gssgfbull.166.4.375

Teixell, A., Labaume, P., & Lagabrielle, Y. (2016). The crustal evolution of the west-central Pyrenees revisited: Inferences from a new kinematic scenario. Comptes Rendus. Géoscience, 348(3-4), 257-267. https://doi.org/10.1016/j.crte.2015.10.010

Ternois, S. (2019). Reconstruction de la dynamique précoce d'un orogène. Mise en évidence de la transition rifting-collision dans le système est-pyrénéen (France) par la géo-thermochronologie Université de Lorraine].

Ternois, S., Odlum, M., Ford, M., Pik, R., Stockli, D., Tibari, B., Vacherat, A., & Bernard, V. (2019). Thermochronological Evidence of Early Orogenesis, Eastern Pyrenees, France. Tectonics, 38(4), 1308-1336. https://doi.org/10.1029/2018tc005254

Tofelde, S., Bernhardt, A., Guerit, L., & Romans, B. W. (2021). Times Associated With Source-to-Sink Propagation of Environmental Signals During Landscape Transience. Frontiers in Earth Science, 9. https://doi.org/10.3389/feart.2021.628315

Vaucher, R., Musajo, C., Spangenberg, J. E., Poyatos-Moré, M., Zeeden, C., Puigdefàbregas, C., Prieur, M., Castelltort, S., & Adatte, T. (2024). Sediment supply variation control on Lower Eocene delta sequences (Tremp Basin, Spain). Geology. https://doi.org/10.1130/G52548.1

Vauchez, A., & Barruol, G. (1996). Shear-wave splitting in the

Appalachians and the Pyrenees: importance of the inherited tectonic fabric of the lithosphere. Physics of the Earth and Planetary Interiors, 95, 127-138. https://doi.org/https://doi.org/10.1016/0031-9201(95)03125-1

Verges, J., Millán, H., Roca, E., Muñoz, J. A., & Marzo, M. (1995). Eastern Pyrenees and related foreland basins: pre-, syn-, and post-collisional crust-scale cross-sections. Marine and Petroleum Geology, 12(8), 893-915. https://doi.org/https://doi.org/10.1016/0264-8172(95)98854-X

Vinciguerra, C. (2020). Reconstruction des paléo-drainages des bassins précoces péri-orogéniques (Crétacé terminal-Paléocène) à partir des dépôts fluviatiles dans le système pyrénéen oriental Université Bordeaux Montaigne].

Weissmann, G. S., Hartley, A. J., Scuderi, L. A., Nichols, G. J., Owen, A., Wright, S., Felicia, A. L., Holland, F., & Anaya, F. M. L. (2015). Fluvial geomorphic elements in modern sedimentary basins and their potential preservation in the rock record: A review. Geomorphology, 250, 187-219. https://doi.org/10.1016/j.geomorph.2015.09.005

Westerhold, T., Marwan, N., Drury, A. J., Liebrand, D., Agnini, C., Anagnostou, E., Barnet, J., Bohaty, S., De Vleeschouwer, D., Florindo, F., Frederichs, T., Hodell, D. A., Holbourn, A., Kroon, D., Lauretano, V., Littler, K., Lourens, L. J., Lyle, M. W., Pälike, H., Zachos, J. C. (2020). An astronomically dated record of Earth's climate and its predictability over the last 66 million years. Science, 369(6509), 1383-1387. https://doi.org/10.1126/science.aba6853

Westerhold, T., Röhl, U., Donner, B., & Zachos, J. C. (2018). Global Extent of Early Eocene Hyperthermal Events: A New Pacific Benthic Foraminiferal Isotope Record From Shatsky Rise (ODP Site 1209). Paleoceanography and Paleoclimatology, 33(6), 626-642. https://doi.org/10.1029/2017pa003306

Whipple, K. X., & Tucker, G. E. (1999). Dynamics of the stream-power river incision model: Implications for height limits of mountain ranges, landscape response timescales, and research needs. Journal of Geophysical Research: Solid Earth, 104(B8), 17661-17674. https://doi.org/10.1029/1999jb900120

Whitchurch, A. L., Carter, A., Sinclair, H. D., Duller, R. A., Whittaker, A. C., & Allen, P. A. (2011). Sediment routing system evolution within a diachronously uplifting orogen: Insights from detrital zircon thermochronological analyses from the South-Central Pyrenees. American Journal of Science, 311(5), 442-482. https://doi.org/10.2475/05.2011.03

Whittaker, A. C., Duller, R. A., Springett, J., Smithells, R. A., Whitchurch, A. L., & Allen, P. A. (2011). Decoding downstream trends in stratigraphic grain size as a function of tectonic subsidence and sediment supply. Geological Society of America Bulletin, 123(7-8), 1363-1382. https://doi.org/10.1130/b30351.1

Zachos, J. C., Dickens, G. R., & Zeebe, R. E. (2008). An early Cenozoic perspective on greenhouse warming and carbon-cycle dynamics. Nature, 451(7176), 279-283. https://doi.org/10.1038/nature06588

Zachos, J. C., Pagani, M., Sloan, L. C., Thomas, E., & Billups, K. (2001). Trends, rythms, and aberrations in global climate 65 Ma to present. Science, 292, 686-693. https://doi.org/10.1126/science.1059412

Zachos, J. C., Röhl, U., Schellenberg, A., Sluijs, A., Hodell, D. A., Kelly, D. C., Thomas, E., Nicolo, M. J., Raffi, I., Lourens, L. J., McCarren, H. K., & Kroon, D. (2005). Rapid acidification of the ocean during the Paleocene-Eocene Thermal Maximum. Science, 308, 1611-1615. https://doi.org/10.1126/science.1109004

Supplementary Materials

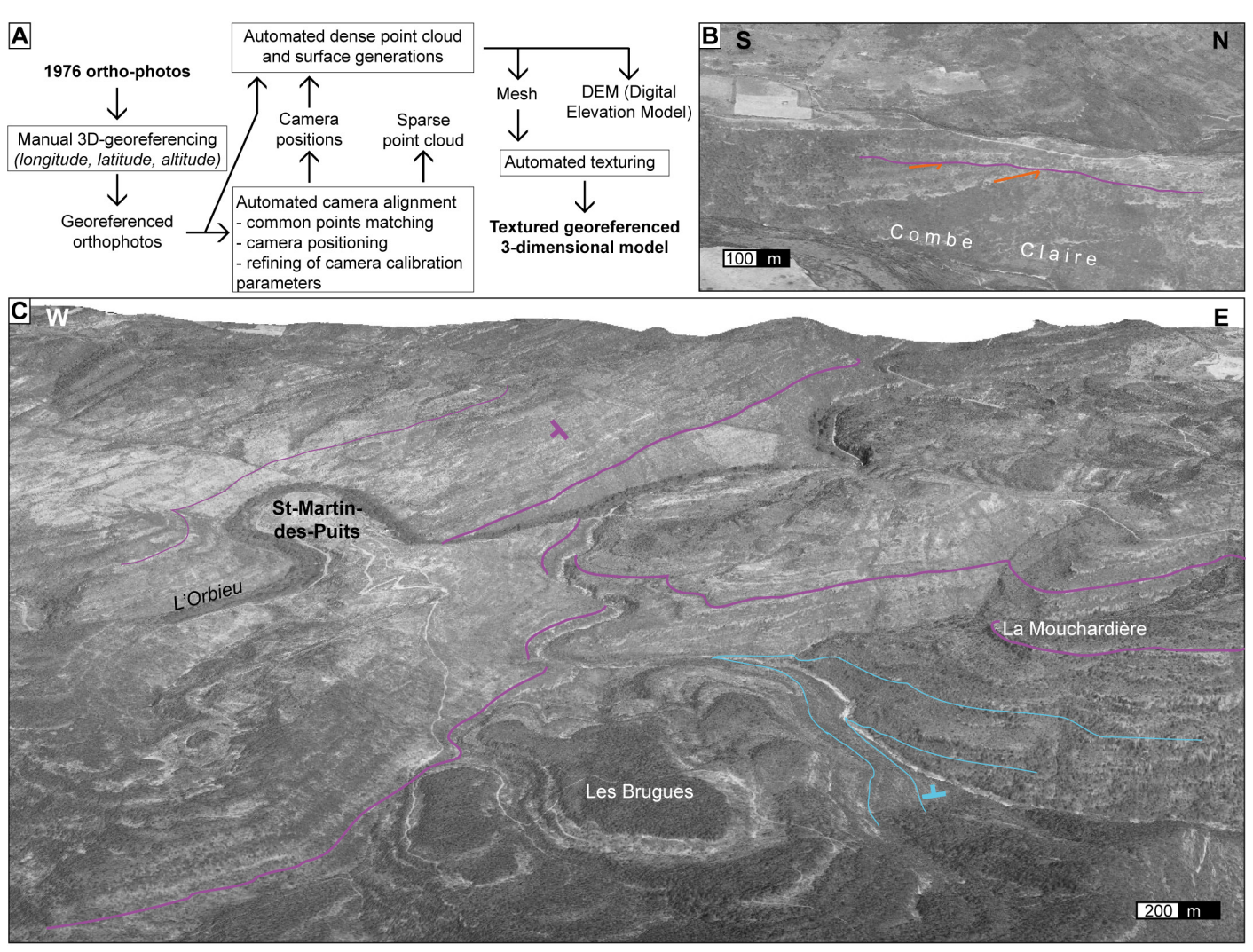


Figure S1: Photogrammetry-based 3D model of the area. (A) Simplified IBR workflow. The 3D model, built from 1976 orthophotos, allows to identify: (B) erosional surfaces and (C) dip variations. Views from Agisoft Metashape Professional.

Table S1: Facies descriptions. Deposits from the Palassou First Unit are described through 11 facies labelled from F1 to F11.

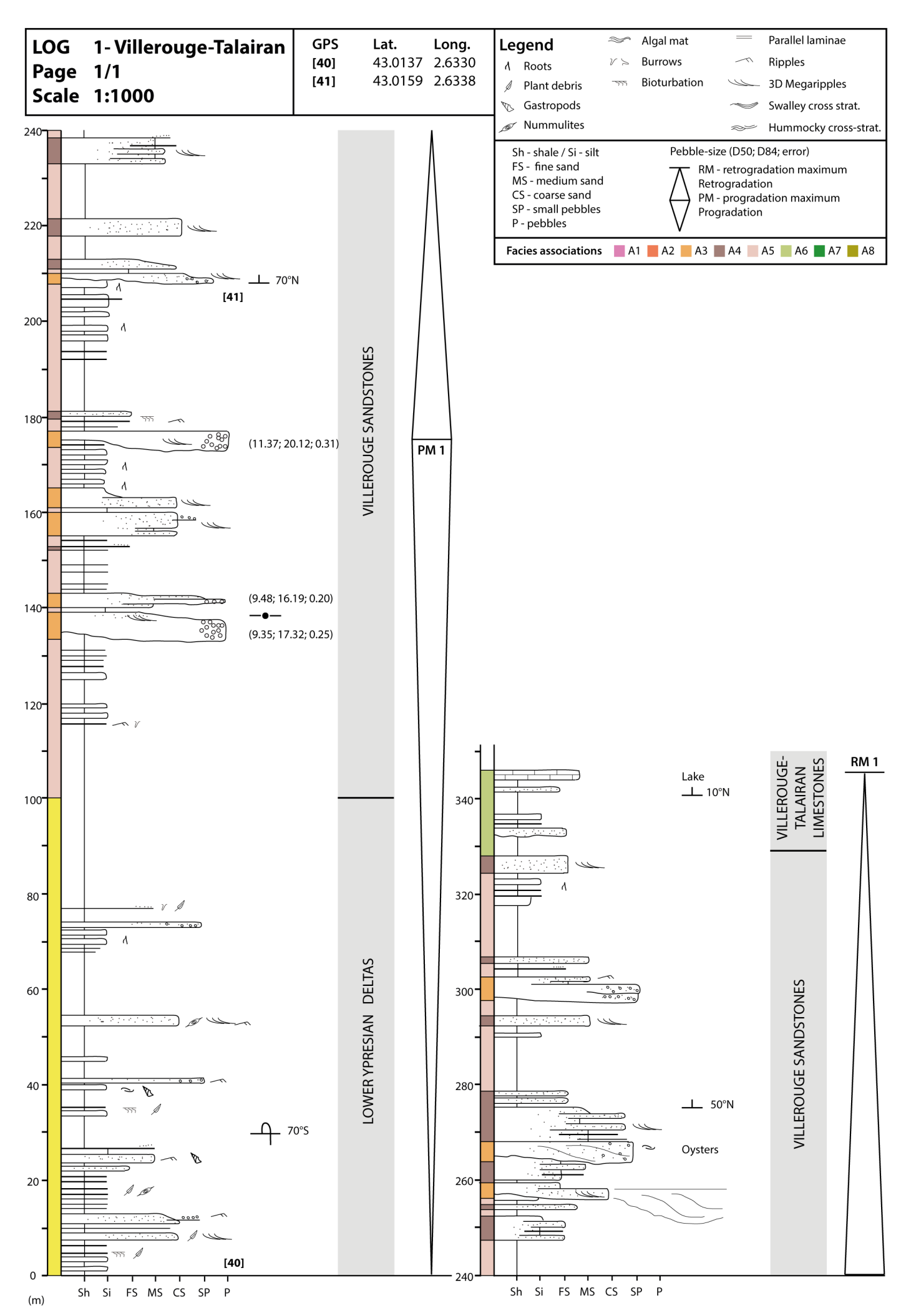
Code	Lithology	Geometry	Structures and Elements	Depositional Environment / process	
F1	Clay / silt alternation	<1m thick silt layers	Roots, mottling, plant debris	Aerial with vegetation - Paleosol	
F2	Silt to very fine sandstone	<1m thick Alternating with clay	Bioturbation, roots, plant debris, rare current ripples	Sub-aerial with vegetation - Hydromorphic paleosol	
F3	Fine sandstone to packstone	≤1m thick	Numerous gastropods, plant debris and algae, plane lamination, some wave ripples	Decantation in shallow waters with biologic activity and rare waves	
F4	Mudstone	<1m thick Limited lateral extent	Biological elements, some bioturbation	Decantation in shallow waters with biologic activity	
F5	Medium/coarse sandstone with floating gravels to unsorted pebbles	≤1m thick Plane and sharp base, locally erosive	None	Fine load within ephemeral unconfined current	
F6	Poorly sorted conglomerates with muddy matrix	0.1-5m thick Sharp base	Some coarsening upward trends	Coarse load within ephemeral unconfined debris flow	
F7	Poorly sorted conglomerates with sandy matrix	1-5m thick Erosive base, sometimes channelized	Interfingering of internal erosional surfaces, fining upward trends	Coarse load within periodic high energy current	

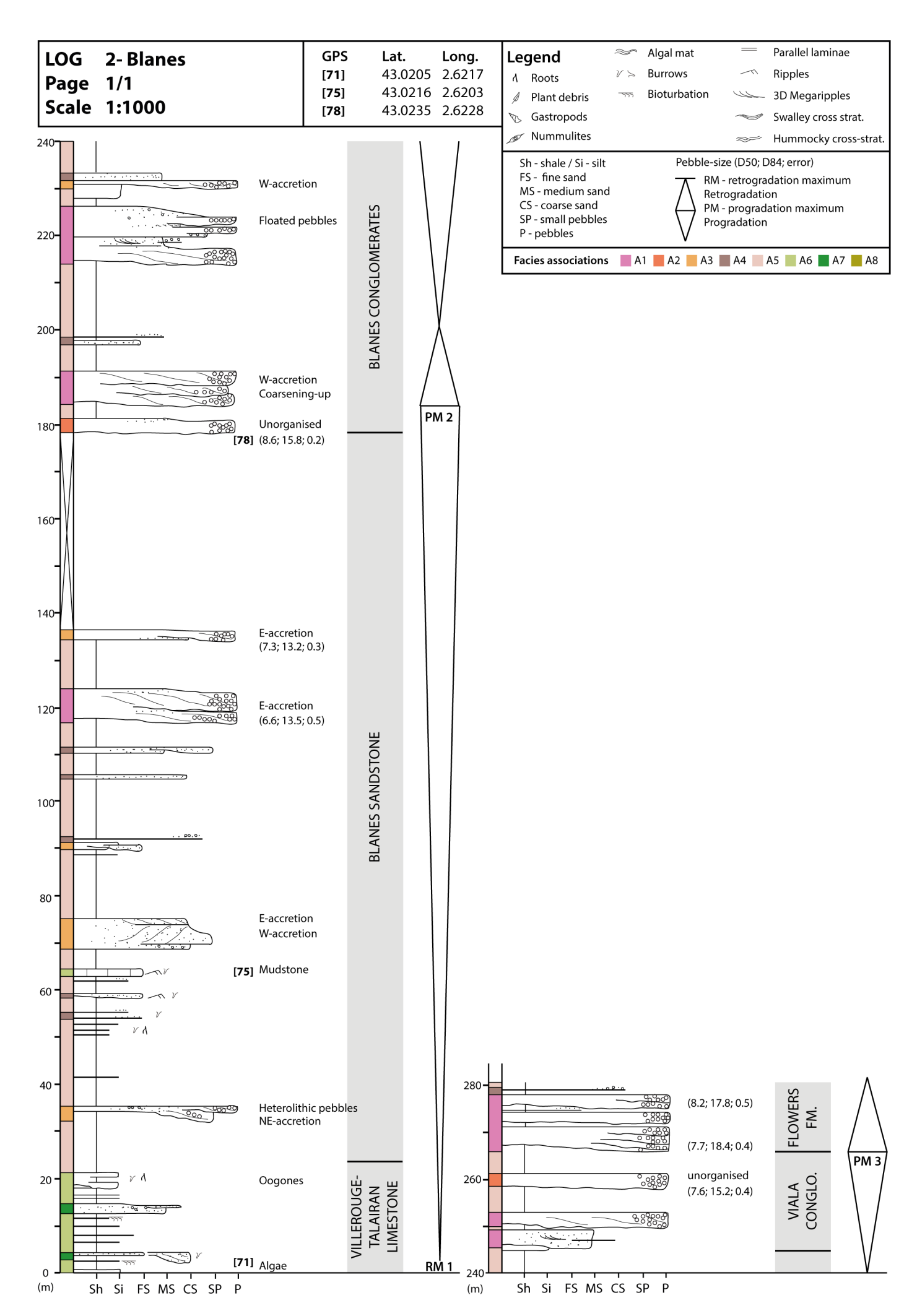
Code	Lithology	Geometry	Structures and Elements	Depositional Environment / process
F8	Sandstone to conglomerates with sandy matrix	1-5m thick Sharp base, locally erosive	Humpback cross-beds	Ephemeral upper flow regime
F9	Fine to coarse sandstone with aligned gravels	≤1m thick Plane and sharp base, locally erosive. Alternating with clay and silt. Lateral of F11	Current ripples, fining upward trends, plant debris, bioturbation on top	Fine load within ephemeral, unconfined and tractional current - Crevasse splay
F10	Fine to coarse sandstone	≤1m thick Often overlying on F11	Abundant current ripples and 3D megaripples	Fine load within continued, channelized and tractional current
F11	Coarse sandstone to conglomerates with sandy matrix	Large foresets Erosive channelized lenses, amalgamated or isolated in clay and silts	Aligned pebbles, some imbrications, fining upward trends	Coarse load within conti- nued, channelized, high energy tractional current

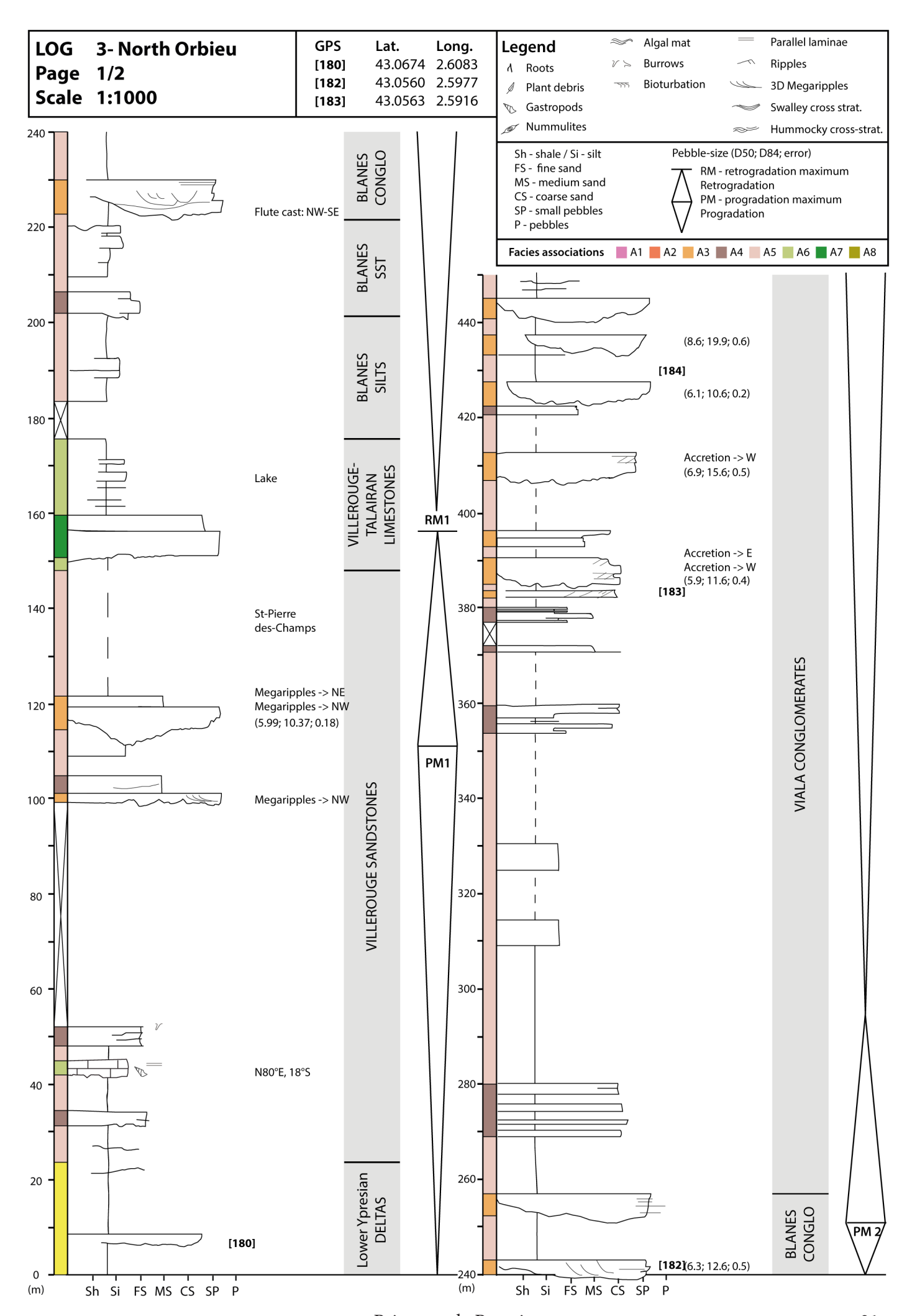
Table S2: Facies associations descriptions. Facies are grouped into 8 facies associations, labelled from A1 to A8, with different frequencies from proximal to distal.

Code	Name	Associated facies	Description	Frequency and proximal - distal polarity		
A1	Amalgamated conglomeratic channels	F6; F7; F11	Large body of poorly sorted conglomerates with discernable channel lenses and some foresets. Highly erosional.	High frequency Most-proximal		
A2	Unorganised conglomeratic channels	F5; F6, F7; F8	Isolated coarse-grained channels with barely no structure except raremarkers of upper flow regime	Low frequency Most-proximal		
A3	Isolated channels	F10; F11 Lateral variation: A4 Interbedded with A5	Channel lenses with lateral accretion overlied by fine sandstone with megaripples	High frequency Proximal to distal, with downstream decrease in grain size and channel dimensions		
A4	Crevasse splay	F9 Lateral variation: A3 Interbedded with A5	Coarsening up sandstones deposited in floodplain deposits during floods, laterally to isolated channels	High frequency, increasing down-system.		
A5	Paleosols	F1; F2	Pedogenic clay and silts with rootlets	High frequency, increasing down-system		
A6	Lacustrine	F2; F3; F4	Carbonated to sandy, more or less laterally continuous, with high biologic content and some current structures	Low frequency Oxbow lakes if low lateral continuity (above A3) Distal ephemeral lakes if laterally continuous (in- terbedded with A5)		
A7	Lacustrine delta	F10; F11 Interbedded with A6	Coarse tractionnal cur- rents within lacustrine fine deposits	Low frequency Distal lakes		
A8	Lacustrine turbidites	F5; F6 Interbedded with A6	Coarse gravity flows within lacustrine fine deposits	Low frequency Distal lakes		

Figure S2 (following pages): Detailed logs. (L1) Villerouge-Talairan. (L2) Blanes. (L3) North Orbieu. (L4) South Orbieu. (L5) St Martin - Jonquières. (L6) Hautes Jonquières. (L7) Villetritouls. (L8) Labastide-en-Val. (L9) Lairière. (L10) Arquettes-en-Val. (L11) La Vène. (L12) Ladern-sur-Lauquet. (L13) St Hilaire. (L14) St Polycarpe. (L15) Alcouffe. (L16) Pomas. (L17) Magrie. (L18) Le Bois.

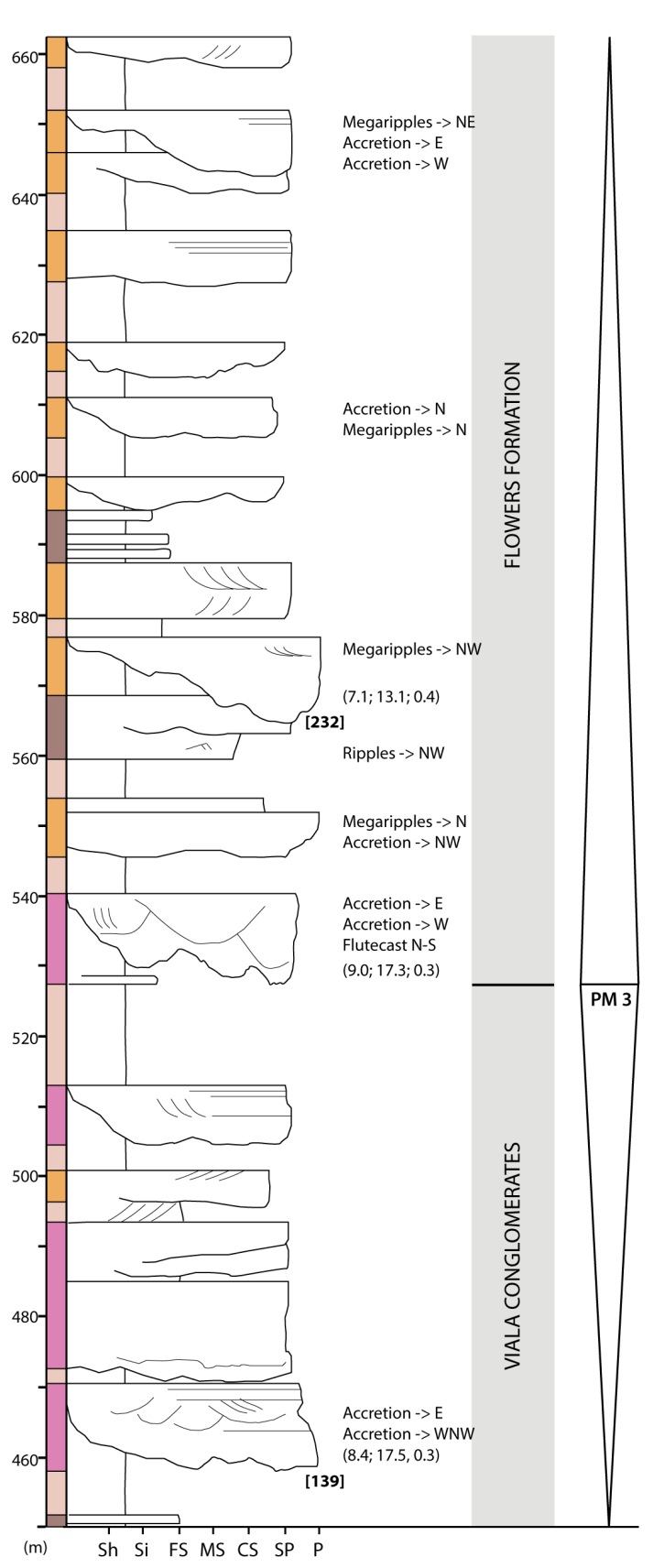


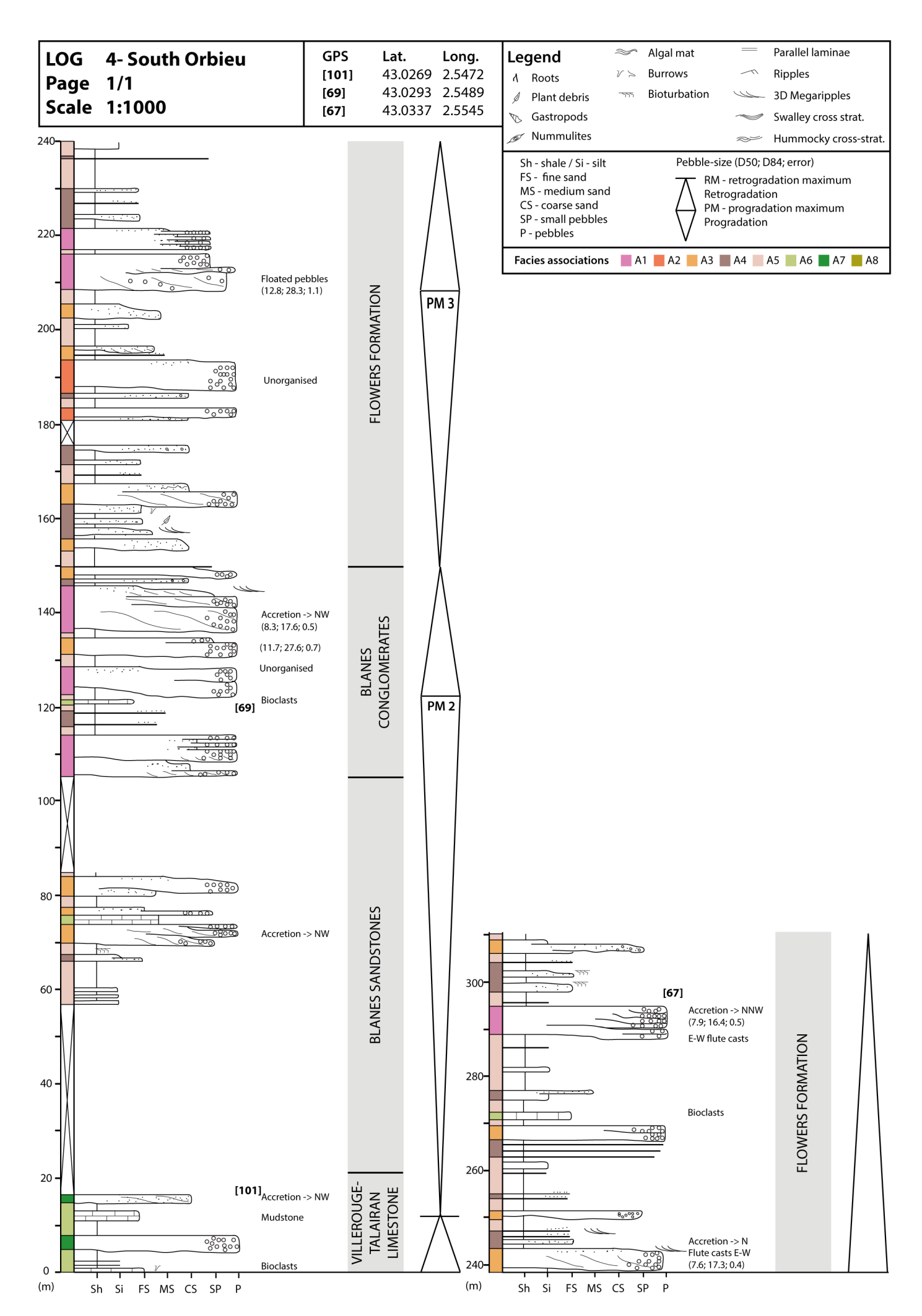


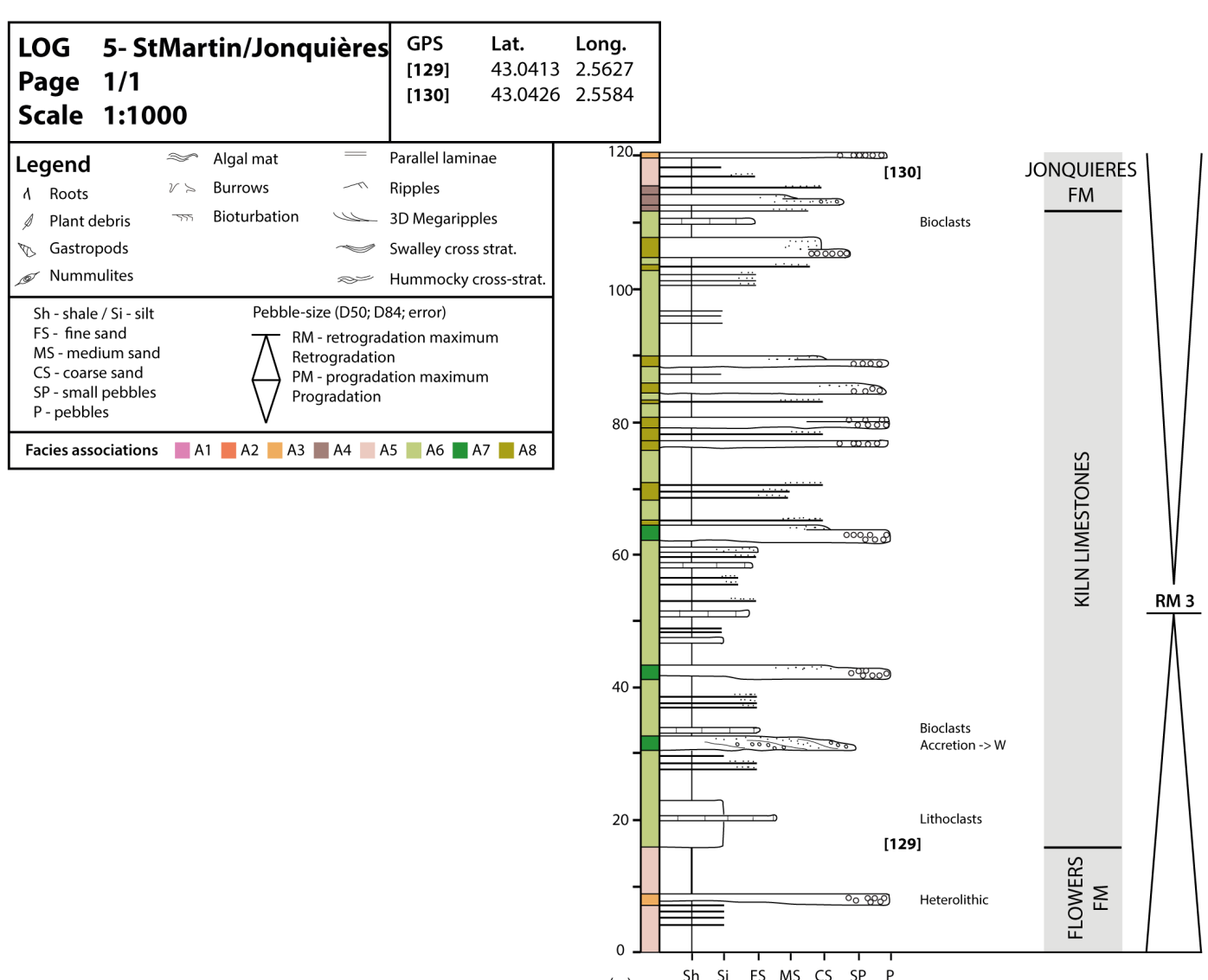


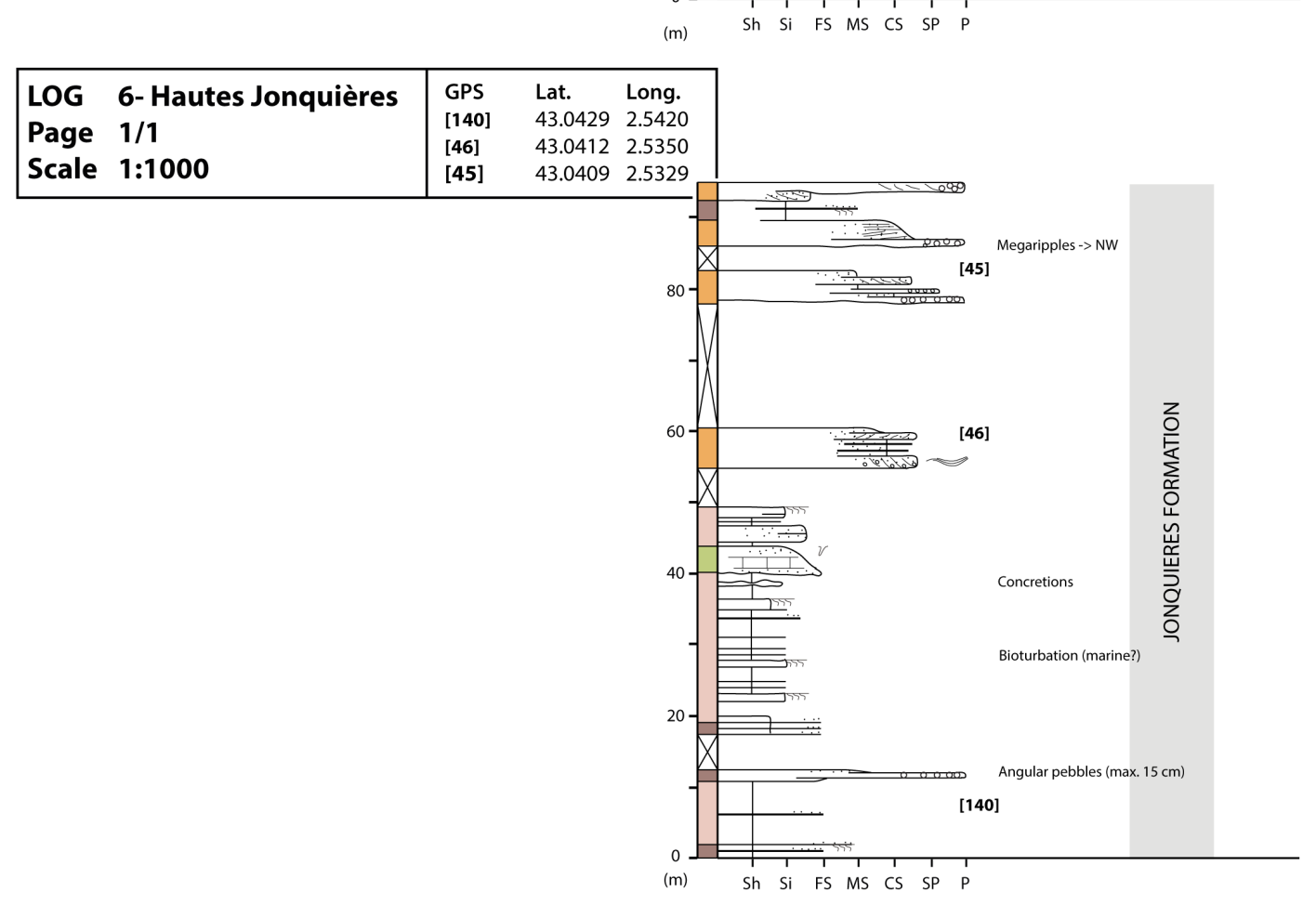
Page	3- North Orbieu 2/2 1:1000	GPS [184] [139] [232]	Lat. 43.0536 43.0434 43.0407	2.5827	Legend ↑ Roots ₱ Plant debris ▼ Gastropods	* 1 ' ' ' ' ' ' ' ' ' ' ' ' ' ' ' ' ' '	Algal mat Burrows Bioturbation		Parallel laminae Ripples 3D Megaripples Swalley cross strat.
					Sh - shale / Si - silt FS - fine sand MS - medium sand CS - coarse sand SP - small pebbles P - pebbles	ht Pebble-size (D50; D84; error) RM - retrogradation maximu Retrogradation PM - progradation maximum		dation maximum on ation maximum	

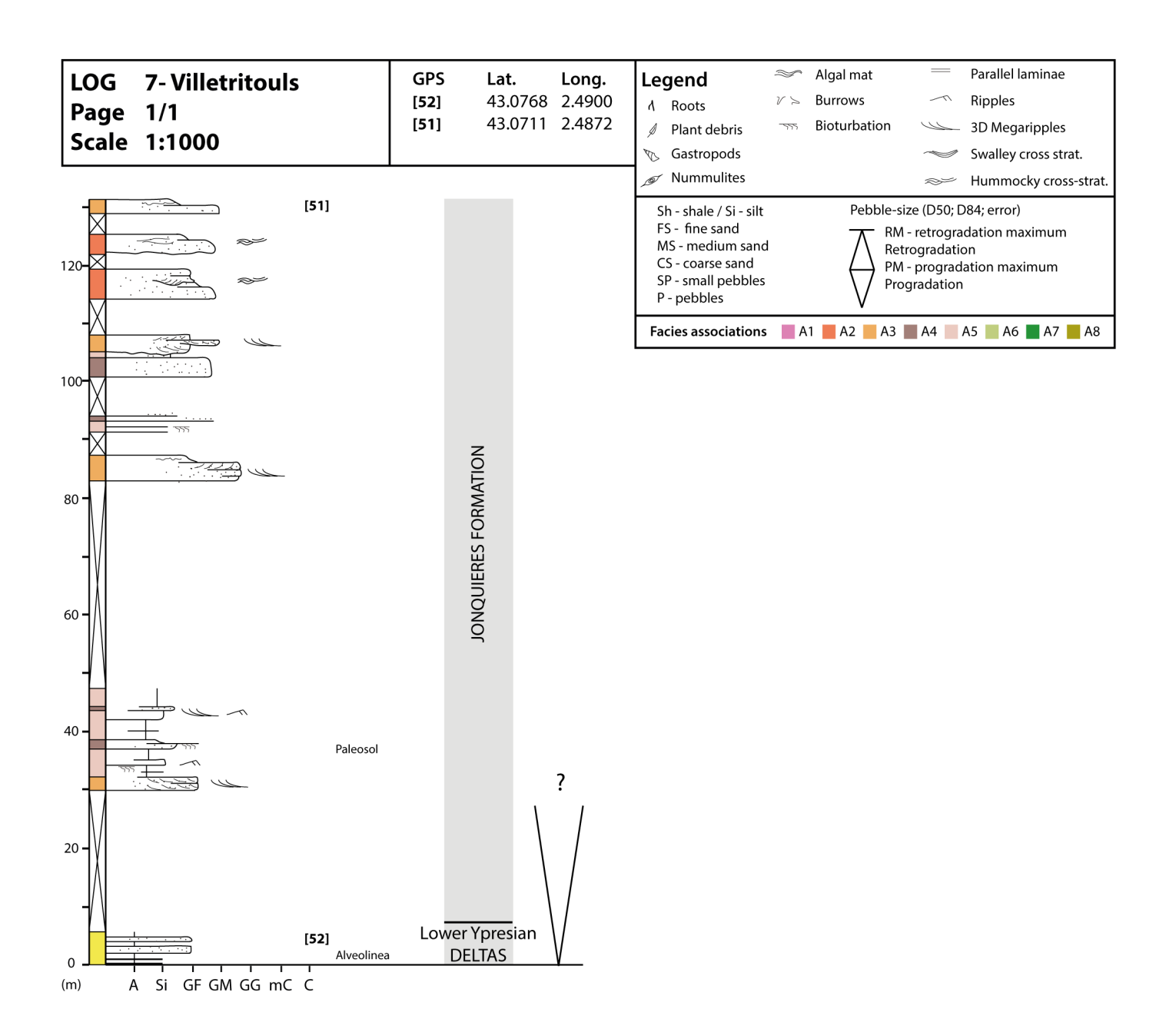
Facies associations A1 A2 A3 A4 A5 A6 A7 A8

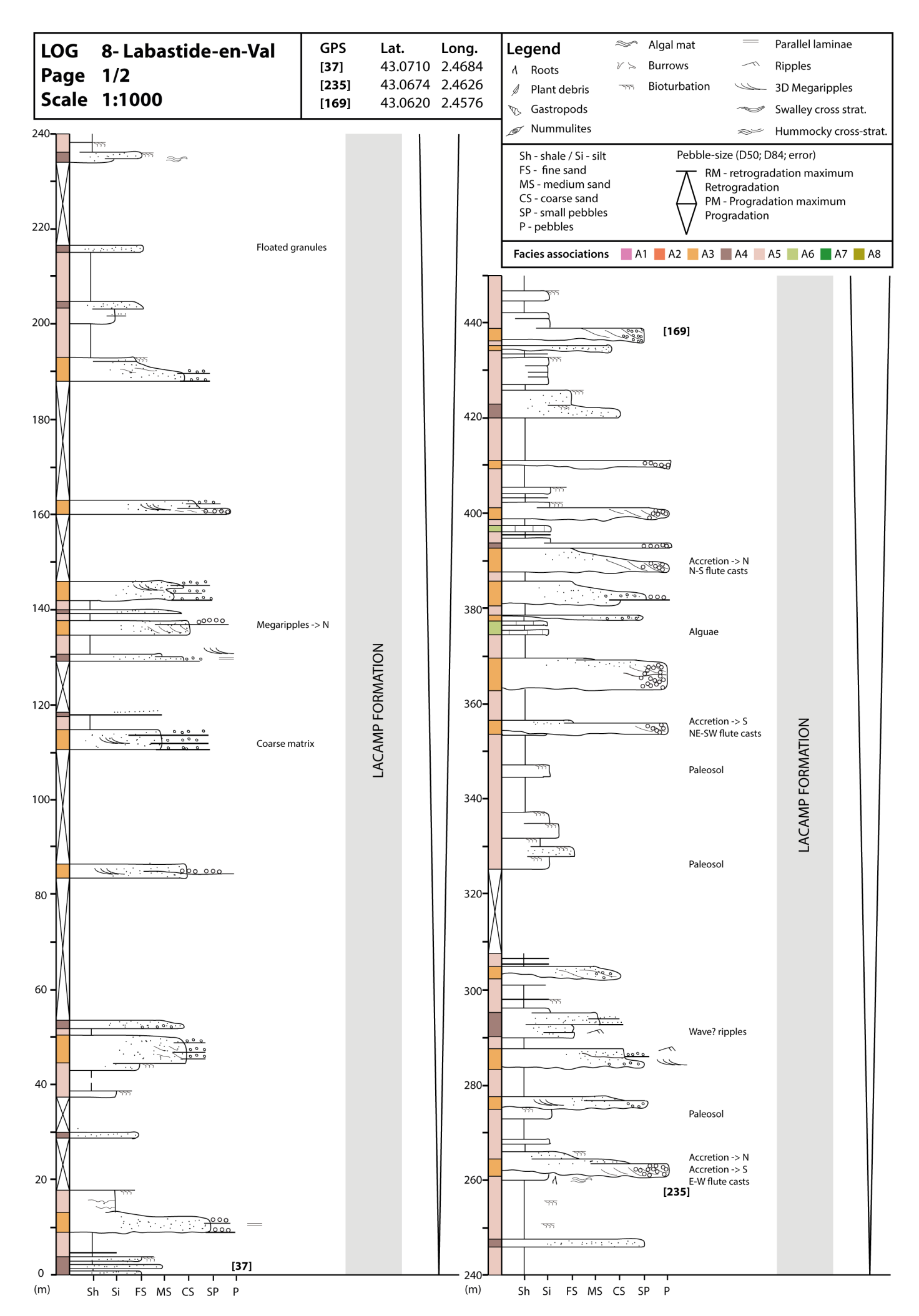


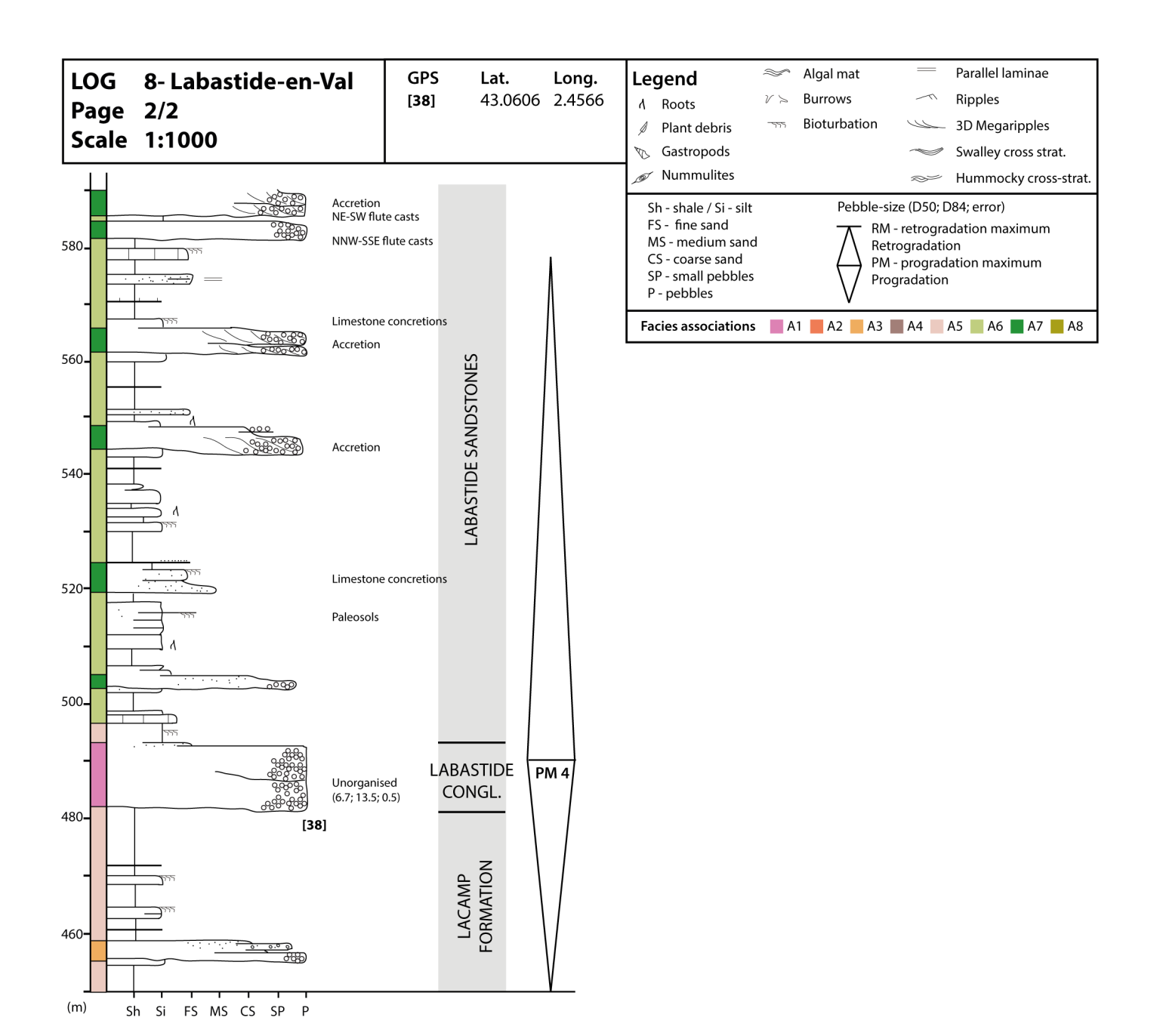


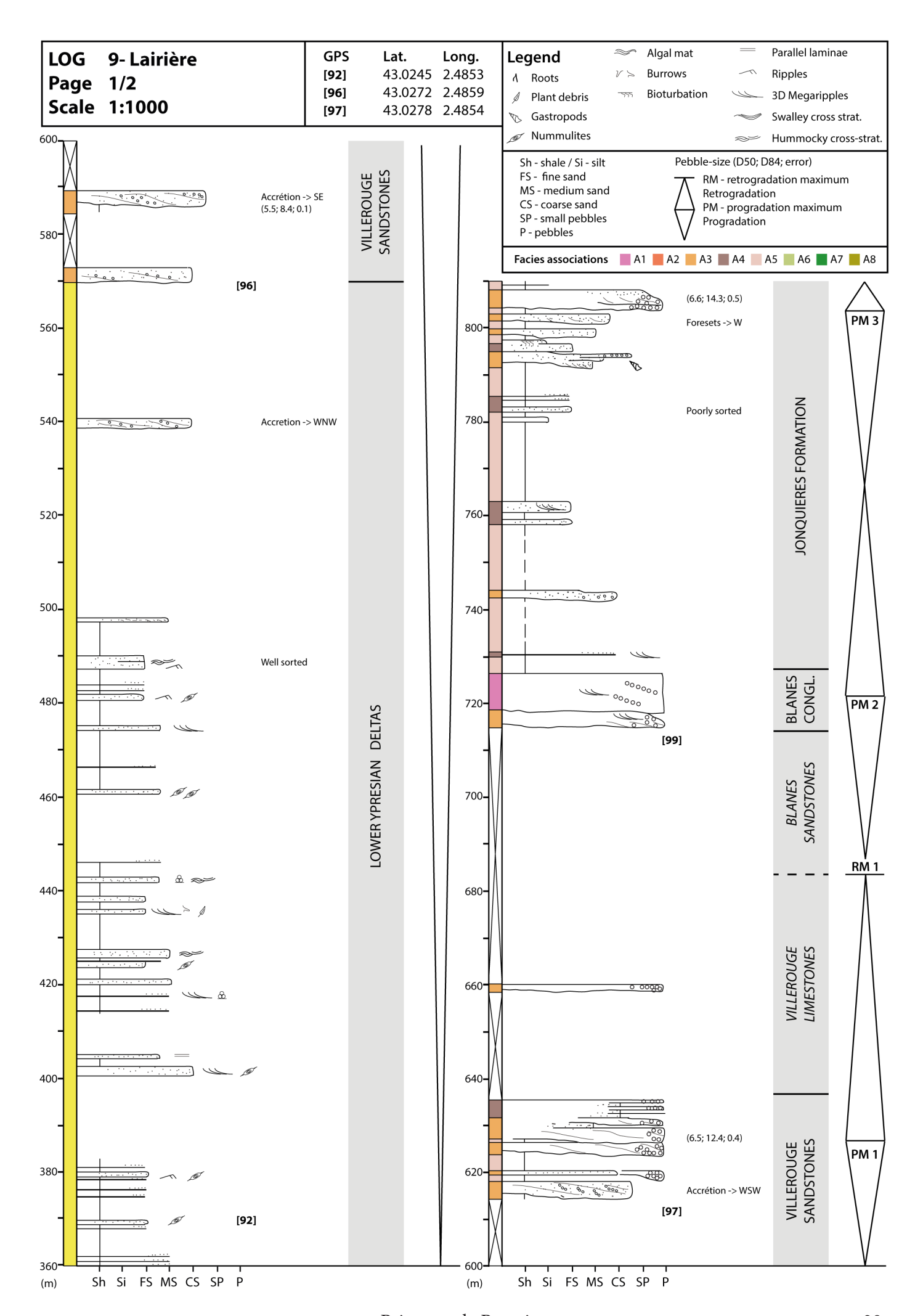


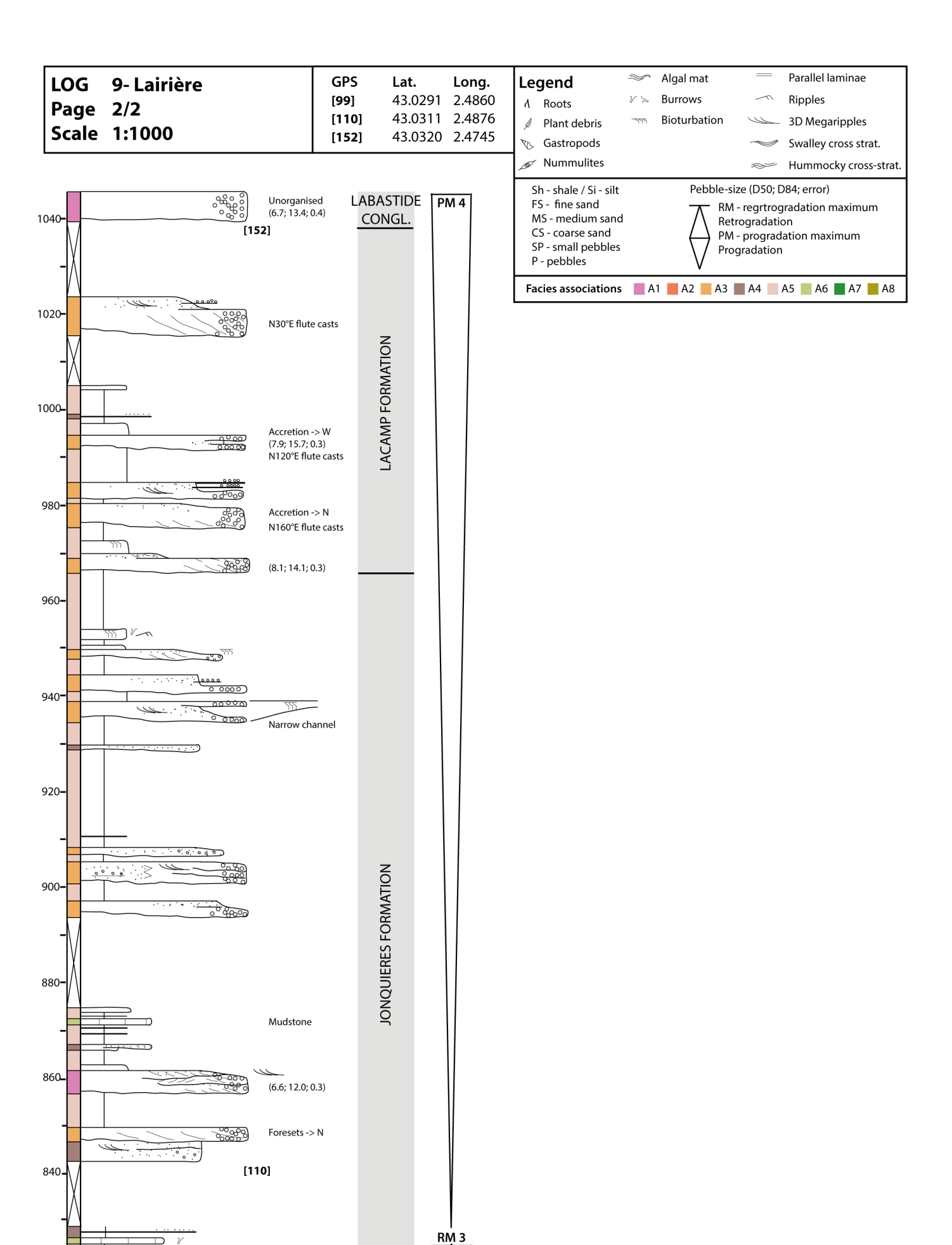












(6.8; 12.7; 0.4)

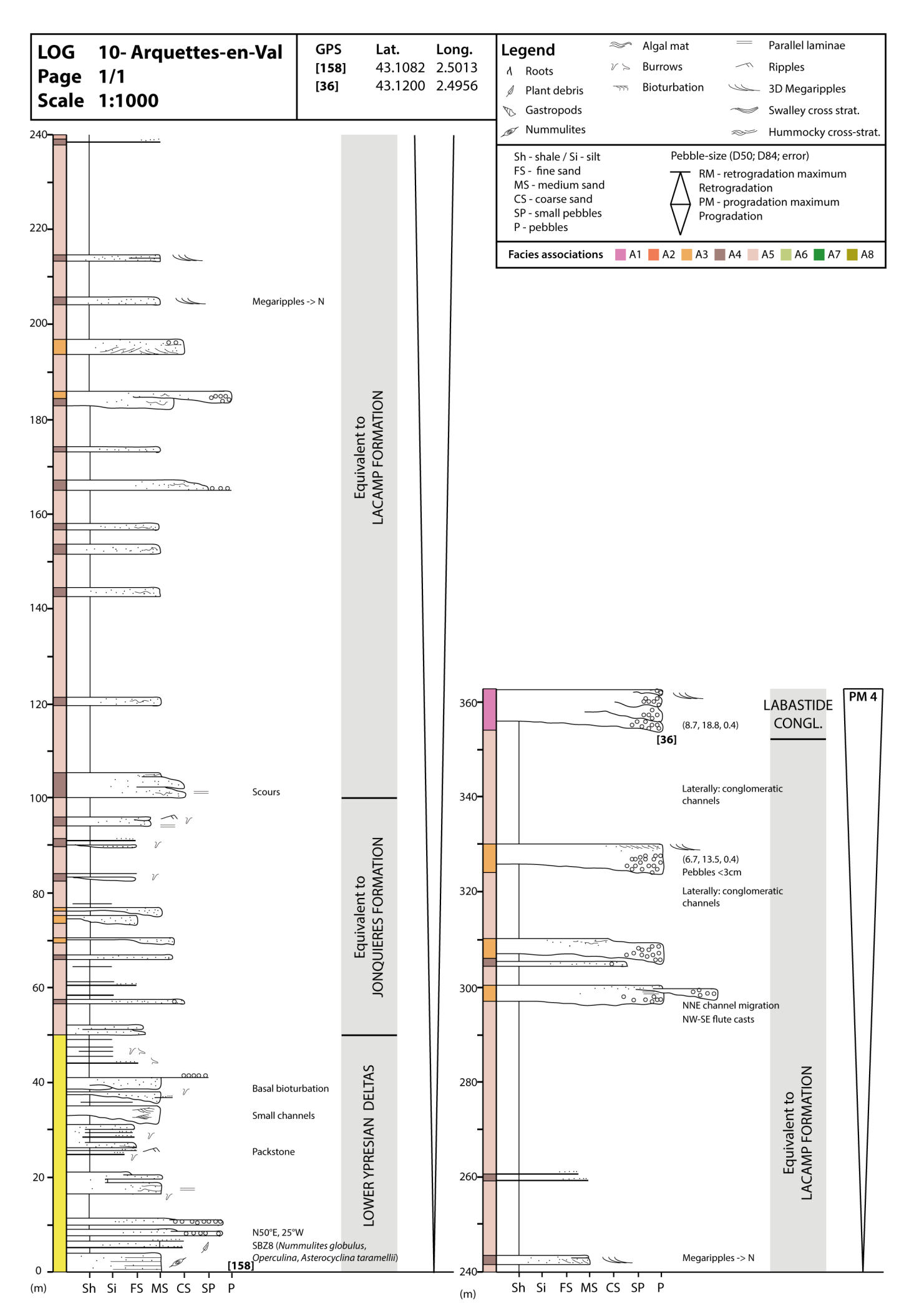
00000

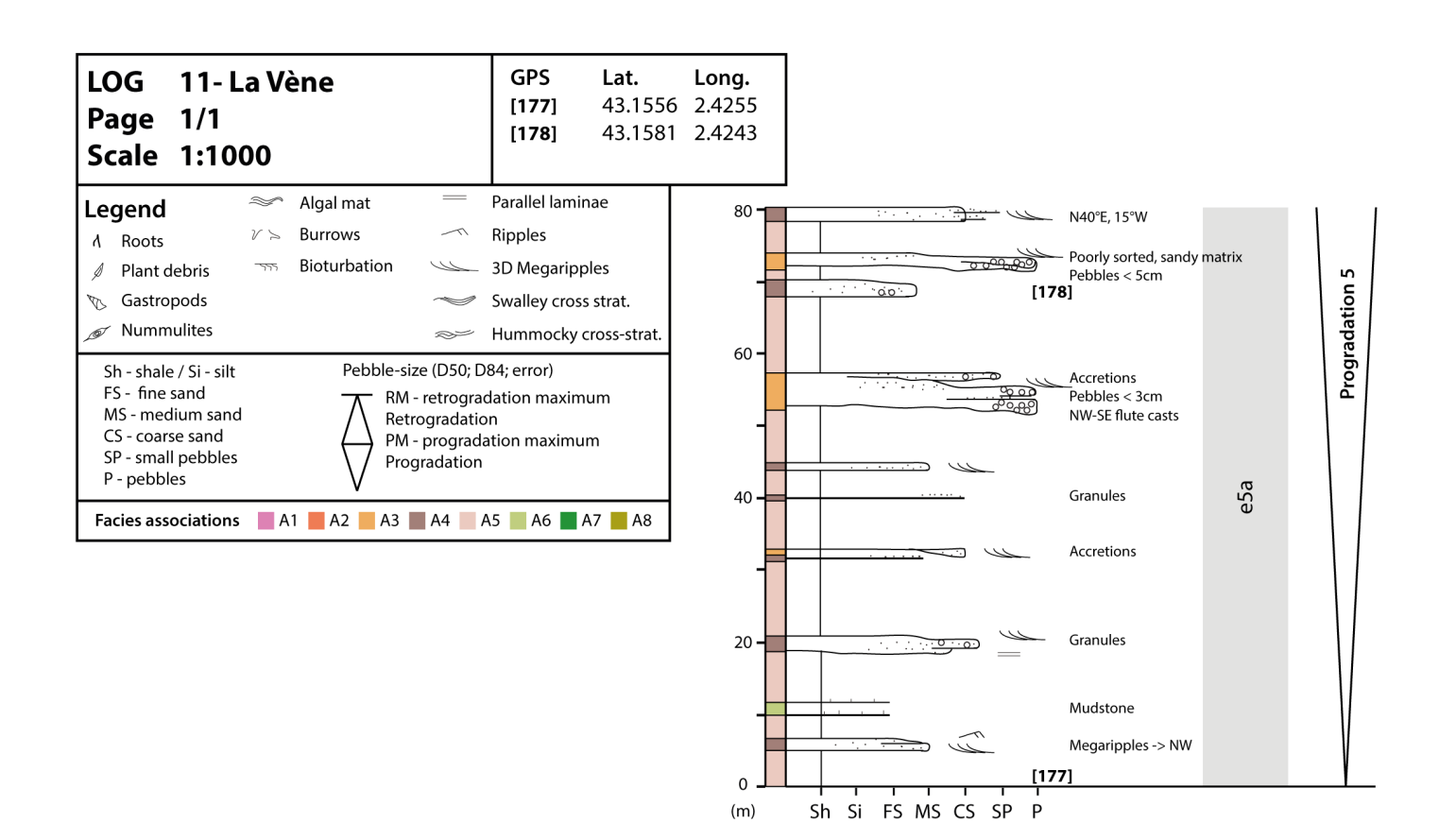
Sh Si FS MS CS SP P

Foresets -> E + W

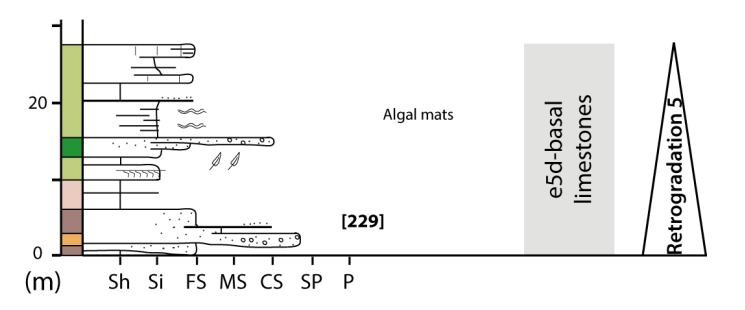
820

(m)





LOG	12- Ladern-s/-Lauquet	GPS		Long.
Page	1/1	[229]	43.1028	2.3584
Scale	1:1000			



LOG	13 Stillalic	GPS	Lat.	Long.
Page	1/1	[35]	43.0904	2.3179
Scale	1:1000			

